Electronics and Computer Science
Faculty of Engineering and Physical Sciences
University of Southampton

Carl Richardson

May 12, 2020

Identifying the Level of Consciousness by Parameter Estimation of an 8-Cell Thalamocortical Network

Project Supervisor: Dr Srinandan Dasmahapatra

Second Examiner: Professor Koushik Maharatna

A project report submitted for the award of
MEng Electronic Engineering with Artificial Intelligence

Abstract

Can the brain state, representing the level of consciousness, be identified from extracellular recordings? An 8-cell model of the thalamocortical region was fitted to the, noisy, observed data by tuning the parameters modified by the general anaesthetic- Propofol. Baseline and strong frontal alpha oscillation brain states were used as case studies; respectively, they modelled the brain in a conscious and unconscious state. As commonly found in biology, multiple models replicated the observed extracellular recordings well and the implications of this were discussed. The decision function measured the similarity between the optimal model and each reference model. The reference model with the best similarity score was identified as the observed brain state. Sensitivity analysis was used to investigate the stability of the optimal models. The results showed, in both case studies, that the optimal model was significantly more sensitive to the GABA conductance parameters compared to the GABA time constant.

Statement of Originality

I, Carl Richardson, declare that this project and the work presented in it is my own and has been generated by me as the result of my own original research. I confirm that:

- I have read and understood the ECS Academic Integrity information and the University's Academic Integrity Guidance for Students.

- I am aware that failure to act in accordance with the Regulations Governing Academic Integrity may lead to the imposition of penalties which, for the most serious cases, may include termination of programme.

- I consent to the University copying and distributing any or all of my work in any form and using third parties (who may be based outside the EU/EEA) to verify whether my work contains plagiarised material, and for quality assurance purposes.

- I have acknowledged all sources, and identified any content taken from elsewhere.

- I have used the following open-sourced code:
  - DifferentialEquations.jl
  - DiffEqParamEstim.jl
  - RecursiveArrayTools.jl
  - Optim.jl
  - LineSearches.jl
  - LinearAlgebra.jl
  - Random.jl
  - DiffEqSensitivity.jl
  - CSV.jl
  - Tables.jl
  - Plots.jl

- I did all the work myself, or with my allocated group, and have not helped anyone else.

- The material in the report is genuine, and I have included all my data/code/designs.

- I have not submitted any part of this work for another assessment.

- My work did not involve human participants, their cells or data, or animals.

Acknowledgments

Firstly, I would like to thank my supervisor Dr Srinandan Dasmahapatra for encouraging me to explore my own interests and providing invaluable guidance throughout the year.

I would also like to acknowledge Christopher Rackauckas and the other contributors for the public release of *DifferentialEquations* and its associated packages. These packages were critical in each stage of the project.

Finally, I would like to thank my family for their unwavering support over the course of this project and long before.

Contents

Table of Figures

1 Introduction

1.1 Context

Computational neuroscience is an approach to understanding how information, in the form of neural signals, is processed in the brain by modelling the nervous system at circuit and system levels. The human brain is a complex network made up of approximately 86 billion neurons [1] where each neuron has, on average, 7 thousand synapses connecting them to other neurons [2]. The complexity of a computational model providing one-to-one mapping of a human's connectome would be way too high to practically be solved with current technology. Simplified models generating data in the same form as current experimental measurement techniques are required for the results to be computed and compared. Techniques such as extracellular recording or cell-attached patch-clamp recording [3] measure the voltage traces of individual neurons. Therefore, models which directly generate each neuron's membrane potential can be used.

The purpose of the model developed in [4] was to simulate the network mechanisms of the thalamocortical region of the brain with and without the effects of the general anaesthetic- Propofol. Variations of the famous Hodgkin and Huxley dynamic equations [5] were used to represent the action potentials and the interactions between the neuron's via synapse currents. The administration of Propofol was implemented in the model by the modification of the GABA receptor dynamics. Specifically, the GABA conductance and decay time parameters were increased proportionally to the dose of Propofol that was administered [4]. The analysis conducted in [4] used the frequency band observed by an EEG reading as a marker for the level of consciousness. It showed this frequency was dependent upon the GABA current and as a result- must be dependent upon the GABA receptor dynamics.

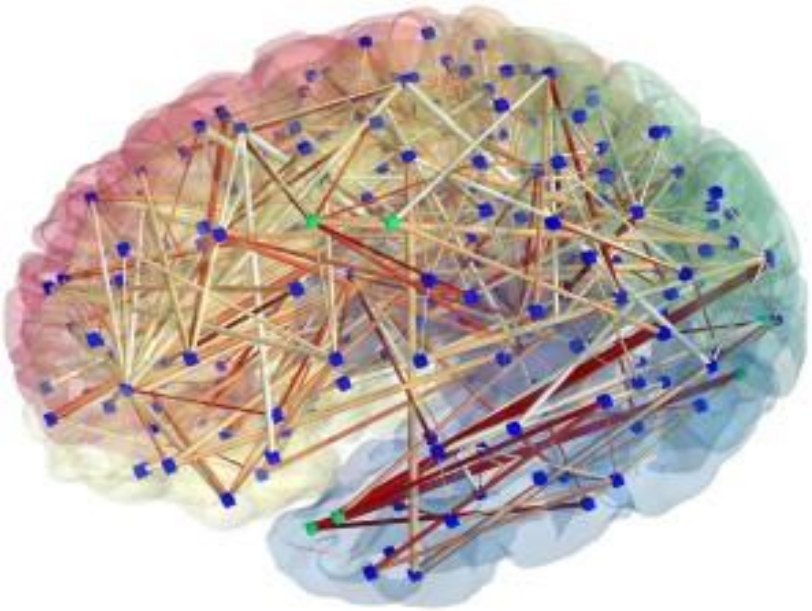

Figure 1: The brain represented as a network [6]

1.2 Scope

The scope of this project was to use machine learning to investigate whether the brain state, representing the level of consciousness, could be inferred from data measured by extracellular recording, or any other procedure with the capability to measure the voltage trace of selected neurons. Based on the findings of [4], the brain state can be inferred from the maximal GABA conductance and decay time. The following framework was used to set up the parameter estimation problem:

1. Implement the model as an autonomous system of differential equations parameterised by the GABA maximal conductance and decay time.
2. Generate training and test data sets by using the model and adding random noise to the data.
3. Derive an objective function dependent upon the system parameters.
4. Minimise the objective function to find the parameter values which best reproduce the observed data.
5. Analyse how well the learnt model fits the test data.

This framework is commonly referred to as an inverse problem within the machine learning context. Many parameter combinations can replicate the observed behaviour well; the meaning of which is extensively discussed in [7]. Further study, in the form of sensitivity analysis, was conducted on the optimal models to examine their stability.

1.3 Report Structure

The report is structured in such a way that reflects the three stages of the project. The first section discusses the implementation of the thalamocortical network and the role of the parameters in shaping the dynamics. The second section focuses on parameter estimation and the third on sensitivity analysis. Whilst reading through these sections, the background research and literature review should be referred to for clarifying some of the fundamental concepts which this project has been built upon.

2 Background Research

2.1 State Space Representation

The 'state' of a dynamical system is the collection of variables that completely characterise the internal and external behaviour of a system [8]. The general form of this representation is known as a state space model and is shown below. The first equation in the model is referred to as the state equation. It is a system of coupled first-order differential equations which represent the dynamics of the state. The second is known as the output equation. The output is the set of variables that can be measured.

$$\frac{d\boldsymbol{x}}{dt} = f(\boldsymbol{x}, t, \boldsymbol{u})$$

Equation 1: State Equation

$$\boldsymbol{y} = h(\boldsymbol{x}, t, \boldsymbol{u})$$

Equation 2:Output Equation

where $\mathbf{x} \in \mathbb{R}^N$ is the state vector, $\mathbf{u} \in \mathbb{R}^M$ is the control/input vector and $\mathbf{y} \in \mathbb{R}^P$ is the output vector.

A special case arises when the state equation does not explicitly depend on **u** or t. In which case, the system is said to be time-invariant or autonomous [8].

$$\frac{d\boldsymbol{x}}{dt} = f(\boldsymbol{x})$$

Equation 3: Autonomous State Equation

In this project, state space representation was used to model the network of neurons sampled from the thalamocortical region of the brain. The model was autonomous and highly non-linear. The state vector included the membrane potentials and the probabilities of the activation/inactivation channels being open for each neuron. When extracellular recording or cell-attached patch-clamp recording was used- the set of membrane potentials comprised the output vector.

2.2 Electrical Properties of a Neuron

The neurons used in the network model were constructed using the Hodgkin and Huxley dynamics [5] as illustrated in figure 2. This removed the spatial dependence of the membrane potential and treated the neuron as a single compartment [9]. This model describes dynamic membrane behaviour seen in all neurons. However, many of the structurally classified neurons used in the network have additional membrane currents incorporated in their models [10].

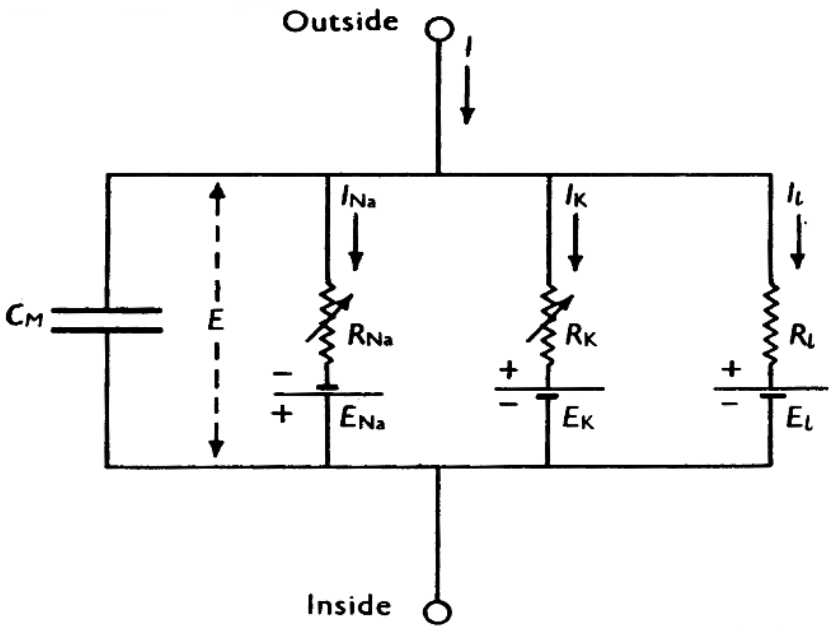

Figure 2: Hodgkin and Huxley model of a neuron [5]

The neuron has excess negative ions inside the cell body, since these repel each other, they build up on the internal surface of the cell membrane [9]. This attracts positive charges to the external surface of the cell membrane causing the cell membrane to behave like a capacitor [9]. The capacitance across the membrane dictates the rate at which the membrane potential (E) can change. This capacitive membrane current is represented by equation 4.

$$i_C = C_M \frac{dE}{dt}$$

Equation 4: Capacitive membrane current

Since "the cell membrane is a lipid bilayer that is impermeable to most charged molecules"; ion channels pass through the membrane at various locations around the cell to allow ions to traverse the membrane [9]. Some channels are chemically controlled, these are located on the dendrites for communicating with other neurons [11]. Other channels are voltage controlled, these are used in the transmission of action potentials [11]. The Hodgkin and Huxley model incorporates two voltage-controlled channels as two parallel branches of the circuit in figure 2. Each branch contains a fixed potential difference (E_{ion}) and a variable resistor. The ions considered in this model are sodium (Na^+) and potassium (K^+). Sodium has a higher concentration outside the neuron whereas potassium has a higher concentration inside the neuron [9]. Naturally, the highly concentrated sodium ions want to diffuse into the neuron whereas the

highly concentrated potassium ions want to diffuse out of the neuron [11]. This behaviour is characterised within the model by including the fixed potential differences (E_{ion}) - the polarity reflects the direction of diffusion. These represent the electrical force required to cancel out the current due to diffusion and are referred to as the equilibrium potential of their respective ion channel. If the membrane potential was equal to an equilibrium potential, no net current would flow through the respective channel.

The variable conductance of each ion channel is dependent upon the membrane potential; hence the channels are modelled by variable resistors [9]. The conductance of each channel is modelled by the maximal conductance of the channel ($\bar{g}$) and all its voltage-dependent activation (m) and inhibition (h) gates [5]. The voltage-dependent gates are described by differential equations where the gating variable takes a value between zero and one. This reflects the openness of the gate, zero being fully closed and 1 being fully open. The general form of these differential equations is shown by equation 5, where u represents the gating variable. u_∞ is the steady state function and τ_u is the time constant of decay [10]. These gating variables are multiplied by the maximal conductance to determine the voltage-dependent conductance of the channel ($\bar{g}m^n h^k$) at any given time. All voltage-controlled channel currents take the general form of equation 6. The sodium channels have 3 activation gates (n=3) and 1 inactivation gate (k=1) and the potassium channels have 4 activation gates (n=4, k=0).

$$\frac{du}{dt} = \frac{u_\infty - u}{\tau_u}$$

Equation 5: Gate equation

$$i_{ion} = \bar{g}m^n h^k (E - E_{ion})$$

Equation 6: Channel current

Some ion channels within the neuron, such as the ion diffusion channels and the ion pumps, have a relatively constant current flow [5]. These channels are grouped as a single constant term and modelled by a constant conductance (g_L). A fixed potential is incorporated into this collective channel to represent the net equilibrium potential of all the channels treated in this way (E_L). These current flows are collectively referred to as the leakage current (i_L) and are described by equation 7.

$$i_L = g_L(E - E_L)$$

Equation 7: Leakage current

The capacitive membrane current is equivalent to the sum of all the channel currents. This includes the ion, leakage and chemically controlled channels. The chemically controlled channels will be discussed later, but for now these currents will be referred to as synaptic currents (i_{syn}). This equation gives rise to the differential equation for the neuronal voltage as shown by equation 8.

$$C_M \frac{dE}{dt} = -\sum i_{ion} - \sum i_{syn} - i_L$$

Equation 8: Neuronal voltage rate equation

2.3 Electrical Properties of a Synapse

Neurons communicate with other cells at a site called the synapse [11]. The neuron that transmits a signal to the synapse is referred to as the presynaptic cell whereas the neuron receiving the signal is known as the postsynaptic cell [11]. Figure 3 shows a neuron connecting to four other neurons via chemical synapses. The gap between the axon terminal (presynaptic terminal) and the dendrite (post synaptic terminal) is called the synaptic cleft [11]. Most synapses in the nervous system are chemical synapses [11]. The presynaptic cell's membrane potential modulates the "release of a neurotransmitter that diffuses across the synaptic cleft and binds to a membrane receptor on the post synaptic cell" [11]. This controls the current flowing through a channel in the membrane.

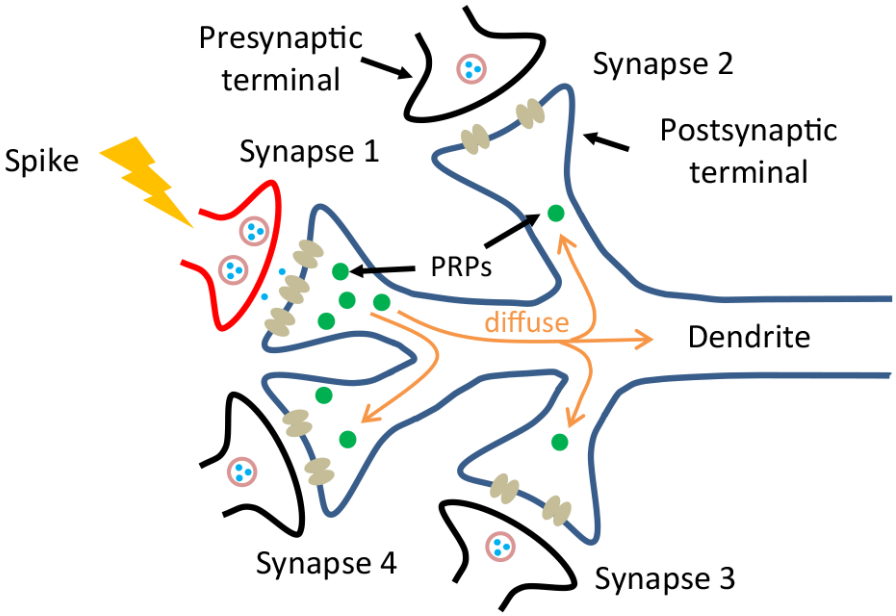

Figure 3: How the presynaptic cell effects the postsynaptic cell when it fires [12]

There is a large array of molecules which act as neurotransmitters throughout the human body. These molecules are grouped into seven classes. Amino acids are one class of molecules which function as neurotransmitters within the central nervous system (CNS) [11]. The neurotransmitters within each class can be classified as excitatory or inhibitory. The excitatory neurotransmitters increase the probability that the postsynaptic cell will trigger an action potential whereas inhibitory neurotransmitters will do the opposite [11]. The excitatory and inhibitory receptors used in the network are AMPA and GABA respectively. The GABA receptor inhibits the probability of an action potential being triggered by allowing chloride ions to hyperpolarise the neuron. The AMPA receptor is a chemically controlled channel which encourages an action potential by allowing sodium, potassium and calcium ions to depolarise the cell [11].

The excitatory and inhibitory synaptic currents are added to the model neuron (figure 2) in the form of two more channels of variable conductance. These are modelled by a variable resistor and a fixed potential difference. The variable conductance of the

AMPA and GABA channels are modelled by their maximal conductance ($\bar{g}_{syn}$) and the gating variable, controlled by the membrane potential of the presynaptic neuron ($s(E_{pre})$), since this controls the neurotransmitters which modulate the conductance of the channels. Equation 9 shows the general form of a synaptic current. E_{syn} represents the diffusion potential of the channel controlled by the GABA or AMPA receptor.

$$i_{syn} = \bar{g}_{syn} s(E_{pre})(E - E_{syn})$$

Equation 9: Synaptic current

2.4 Propofol

"General anaesthesia is a neurophysiological state that consists of unconsciousness, amnesia and immobility" [13]. This state can be persuaded using an anaesthetic such as Propofol. When Propofol is administered, it binds to the post-synaptic GABA receptors of the pyramidal, thalamocortical and thalamic reticular neurons. The sites Propofol bind to are shown in figure 4.

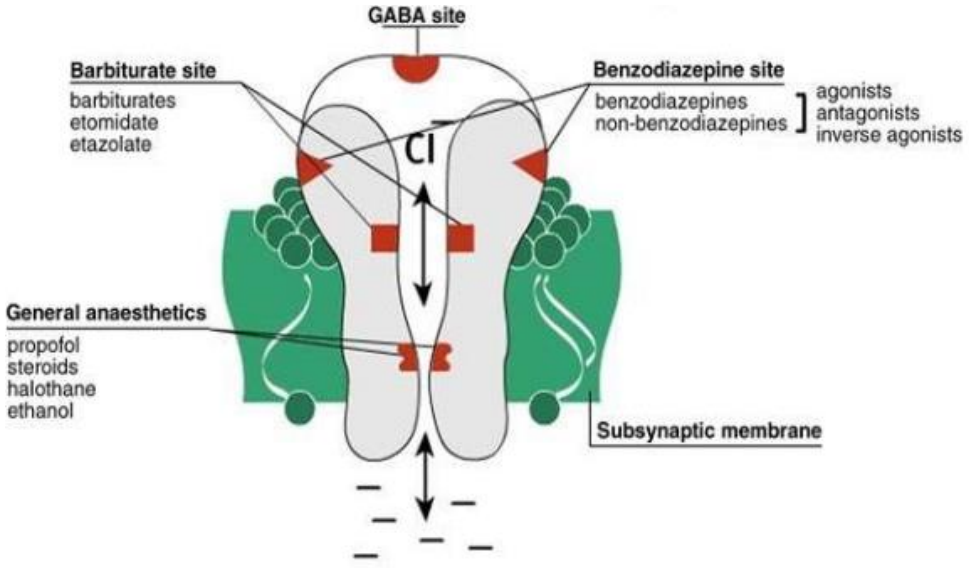

Figure 4: Binding sites on the GABA receptor [14]

When Propofol binds to the GABA receptor, the maximal conductance of the chloride channel increases. Under the same GABA gating variable conditions, more chloride ions flow into the neuron compared to the number of chloride ions without the presence of Propofol. This leads to a greater hyperpolarisation of the cell [15]. Hyperpolarising the cell reduces the probability of an action potential being triggered; hence this current, referred to as a GABA current, is inhibitory [13]. Figure 5 provides an illustration of the difference in the chloride channel's behaviour when Propofol is and is not present at the GABA receptor.

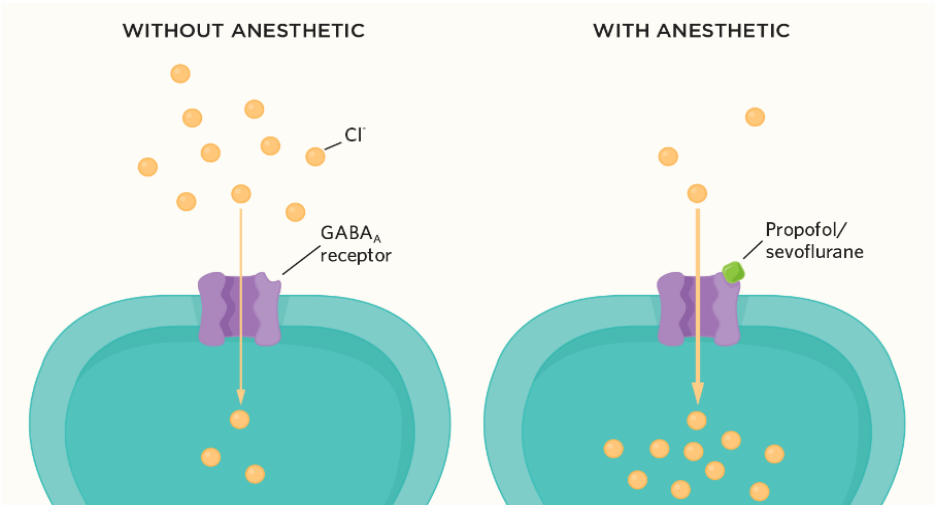

Figure 5: Channel conductance without and with the presence of Propofol [16]

The dynamic effects of Propofol are strongly dependent on the dose and the speed of administration [13]. Since the administration of Propofol modulates the GABA maximal conductance and decay time of the related currents, these parameters shape the dynamics of the network. The state space model of the network is parameterised by these properties to allow the effect of different levels of Propofol to be studied. Associated patterns in the electroencephalogram (EEG) can identify different brain states including: baseline (conscious- no Propofol), paradoxical excitation, strong frontal alpha oscillations, anteriorisation and burst suppression [13]. Low doses of Propofol have the opposite effect of inducing sedation, instead paradoxical excitation is induced [17]. This level of Propofol is not high enough to induce unconsciousness. EEG patterns demonstrating increased power in the beta frequency band (12.5-25 Hz) indicate this excited state [18]. A high dose of Propofol leads to behaviour in the interval of sedation and unconsciousness [19]. Strong frontal alpha oscillations (9-13 Hz) indicate Propofol has induced unconsciousness [20], [21], [22]. Anteriorisation also occurs at high levels of Propofol. Alpha oscillations develop in the anterior region of the brain and as a result, the power in the alpha band increases. At the same time, the alpha oscillations in the posterior region diminish along with the power in the alpha band [20], [22]. Very high doses of Propofol can lead to brain death. Burst suppression patterns exhibit the alternation of high amplitude activity with periods of no activity [19]. This indicates a brain state between unconsciousness and brain death [13].

2.5 Thalamocortical Network

The state space model used was constructed with the smallest set of features necessary to exhibit the spatial and temporal properties outlined in [4], whilst allowing for the manipulation of GABA maximal conductance and decay time to mimic the effects of Propofol. To demonstrate the observed spatial coherence known cortical dynamics were combined with models of the thalamus [4]. These properties identified the network mechanisms associated with different brain states. An 8-cell network using the model neurons and synapses described in [4] met the requirements for this project since it was simple enough to be solved using current technology and could produce data in the form of current experimental measurement techniques. A visual representation of the model is shown in figure 6. The lines with arrowheads represent the AMPA synapses whereas the lines with accents represent the GABA synapses. The arrowhead/accent represent the connection of the synapse to the post-synaptic neuron. Each neuron has the core components discussed in section 2.2, the additional components of each neuron are discussed below.

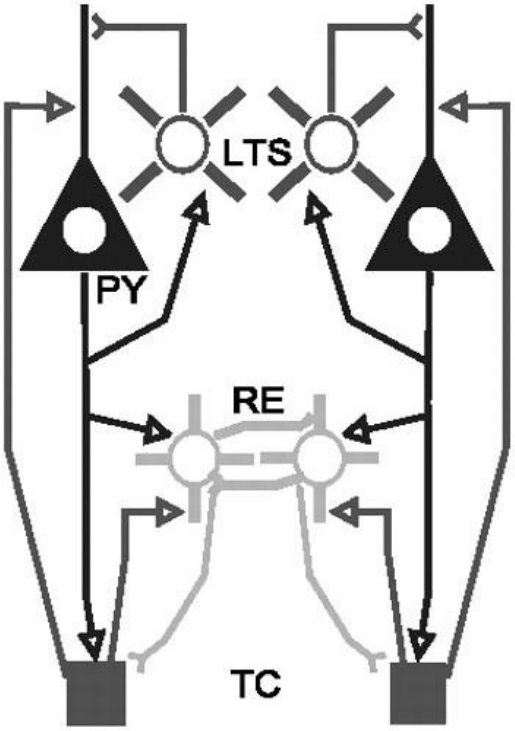

Figure 6: Network model [4]

2.5.1 Pyramidal (PY) Neuron

This neuron contributes to the cortical dynamics of the network. The model of the PY neuron used in [4] has no additional currents added to the basic model neuron described in section 2.2.

2.5.2 Low Threshold Spiking (LTS) Interneuron

This neuron also contributes to the cortical dynamics of the network. The model of the LTS interneuron used in [4] contains an additional M-current added in parallel to the channels of the model neuron described in section 2.2. The M-current is a slow potassium current added to the model to provide the cell with spike frequency adaptation [10]. It takes the form of the channel current shown in equation 6 and has 1 activation gate.

2.5.3 Thalamocortical (TC) Neurons

This neuron contributes to the model of the thalamus. The model used in [4] contains two additional currents added in parallel to the channels of the model neuron described in section 2.2. The T-current takes the form of the channel current shown in equation 6. It is a calcium current activated by negative membrane potentials [4]. It has 2 activation gates and 1 inactivation gate. The h-current is generated from several channels and is involved in 3 key functions [23]:

1. Determination of the resting membrane potential and membrane conductance.
2. Regulation of the response of the neuron to hyperpolarization.
3. The generation of, or contribution to, potentials that control the rate of rhythmic oscillations.

The modelling of this current is more complex and will not be discussed here- for the purpose of this project, the equations from [4] were used.

2.5.4 Thalamic Reticular (RE) Neurons

This neuron makes up the other part of the thalamus model. The model used in [4] contains an extra current added in parallel to the channels of the model neuron described in section 2.2. This extra current is the same T-current described in section 2.5.3.

2.5.5 AMPA Synaptic Connectivity

The network contains two types of synaptic currents which are modelled using the general form of equation 9. The gating variable for the channel controlled by the AMPA receptor is defined by equation 10 [4]. The maximal conductance of the synapse is dependent upon which is the post synaptic neuron.

$$\dot{s}(V_{pre}) = 5\left(1 + \tanh\left(\frac{V_{pre}}{4}\right)\right)(1 - s) - \frac{s}{2}$$

Equation 10: AMPA gating variable

2.5.6 GABA Synaptic Connectivity

When Propofol acts on the network, it modifies the parameters of the GABA synapse- $\bar{g}_{\mathrm{GABA}}$ and τ_{GABA} [4]. The current is modelled using equation 9. The gating variable for the channel controlled by the GABA receptor is defined by equation 11 [4]. The

maximal conductance of the synapse is dependent upon which is the post synaptic neuron.

$$\dot{s}(V_{pre}) = 2\left(1 + \tanh\left(\frac{V_{pre}}{4}\right)\right)(1 - s) - \frac{s}{\tau_{GABA}}$$

Equation 11: GABA gating variable

2.6 L_2-Norm as a Similarity Metric

Consider a matrix $A \in \mathbb{R}^{N\times P}$, the L_2-norm of the matrix is defined by equation 12 [24]. Each element in the matrix has been squared and then square rooted before all being summed together.

$$\left|\left|A\right|\right|_2 = \sum_{i=1}^{N}\sum_{j=1}^{P}\sqrt{a_{ij}^2}$$

Equation 12: L_2-norm of matrix A

This can be used to measure the similarity between 2 matrices. Consider matrices $B \in \mathbb{R}^{N\times P}$ and $C \in \mathbb{R}^{N\times P}$. The L_2-norm of the matrix $B - C$ would be defined by equation 13.

$$\left|\left|B - C\right|\right|_2 = \sum_{i=1}^{N}\sum_{j=1}^{P}\sqrt{(b-c)_{ij}^2}$$

Equation 13: L_2-norm of matrix B-C

The L_2-norm of the difference between 2 matrices calculates the positive difference between each corresponding element of the matrices and sums them all together. The square of the L_2-norm can be written using the inner product matrix notation shown by equation 14.

$$\left|\left|B - C\right|\right|_2^{\,2} = (B-C)^T(B-C)$$

Equation 14: Square L_2-norm in matrix notation

For 2 matrices to be similar, the values of the corresponding elements must be similar [24]. Therefore, the L_2-norm and the square L_2-norm can both be used as similarity metrics. The lower the value of either metric, the greater the similarity between the 2 matrices. For example, if matrix B was equal to matrix C, the L_2-norm would equal zero. The squared L_2-norm was used in this project as the metric for deriving the objective function which was analysed during parameter estimation.

2.7 Optimization- BFGS Method

The BFGS method falls under the umbrella of numerical optimization techniques called Quasi-Newton methods. These methods require only the gradient of the objective function to be supplied at each iterate. The changes in gradients between each iterate are used to construct a model of the objective function that is good enough to produce super linear convergence [25]. This property is used to halt the algorithm when it reaches a local optimum.

The algorithm is defined by [25] as follows:

Given starting point x_0, convergence tolerance $\varepsilon \geq 0$ and inverse Hessian approximation H_0;

$k \leftarrow 0$;

While $\left|\left|\nabla f_k\right|\right| > \varepsilon$ *;*

Compute search direction: $p_k = -H_k \nabla f_k$*;*

Set $x_{k+1} = x_k + \alpha_k p_k$ *where* α_k *is computed from a line search procedure such as* $p_k^T \nabla f(x_k + \alpha_k p_k) = 0$*;*

Define $s_k = x_{k+1} - x_k$ *and* $y_k = \nabla f_{k+1} - \nabla f_k$*;*

Update inverse Hessian approximation by solving $H_{k+1} y_k = s_k$*;*

$k \leftarrow k + 1$*;*

end (while)

The iterative scheme repeats while the magnitude of the objective function's gradient is greater than the convergence tolerance. The independent variable of the objective function, x_k, is found to be the local optimum when this condition is no longer satisfied. This algorithm was used during parameter estimation to find the local minimum of the objective function.

2.8 Evaluating a Population of Models

"An increasing number of studies have shown that the relationship between the parameters of a model and its output can be degenerate; that is, there can be multiple sets of parameters that give rise to the same (or similar) behaviours" [7]. Previous studies, such as [26], investigated this by generating large populations of models and examining the ones which produced similar behaviour. A similar investigation was conducted in [27] where a population of over 20 million model neural networks were generated to investigate the range of pyloric rhythms. The models which produced pyloric rhythms, like the observed biological data, were filtered out. From the 20,250,000 generated models, 452,516 produced pyloric rhythms.

A study into the relationship between sets of neuron parameters, which produced similar voltage traces in model LP neurons, was conducted in [7]. The study quantified the contribution of each model parameter to different network behaviours. The study concluded that a specific spike rate could be generated by a population of models provided a change in one parameter value was compensated for by a change in another. Figure 7 illustrates a range of 2-d parameter distributions which output the same network behaviour. Graph *a* suggests parameters 1 and 2 are statistically independent; in this case, there was no compensation between parameter values. Graph *b* suggests a linear positive correlation and graph *c* suggests a linear negative correlation.

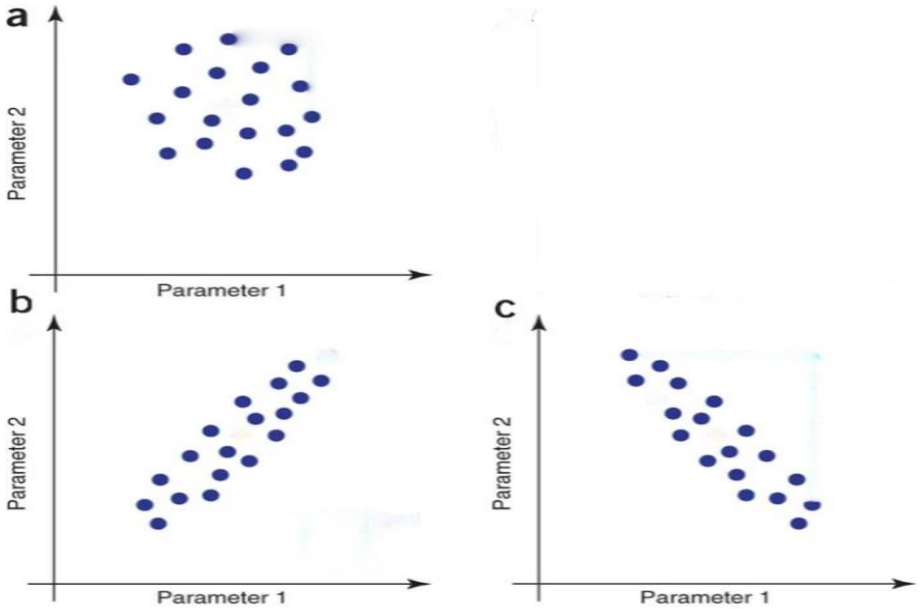

Figure 7: Variety of parameter distributions where all data points output a common behaviour [7]

Furthermore, it was found in [7] that models which produced similar behaviour were generally found in connected regions of parameter space. In higher dimensional parameter spaces, these regions cannot be discovered by looking at a graph, so other methods, such as principle component analysis, must be employed.

3 Modelling the Thalamocortical Network

The focus of this chapter was on modelling the thalamocortical neural network. Given a noisy 8-cell extracellular recording, this model was used for estimating the network parameters modified by Propofol. Using these parameter values, the brain state was identified. The model was also used as the underlying function of the training and test data which random noise was added too. The baseline and strong frontal alpha oscillation brain states were used as case studies since the states represented conscious and unconscious behaviour respectively.

3.1 Choosing a Programming Language

A programming language had to be chosen to implement the state space model of the 8-cell network. This required defining a state space model comprised of 64 state variables which had to be repeatedly solved over a defined time interval. When the parameter estimation problem was accounted for, the number of computations was multiplied by the number of parameter combinations being trialled. Due to the size of the model and the nature of the problem, a high-performance language suitable for numerical analysis was essential.

Three programming languages were considered- Matlab, Python and Julia. A study conducted in [28] performed a comparison of these three languages to be used for implementing global non-linear solution techniques. This study was conducted to evaluate the pros and cons of each language for economists, so economic growth models were used as the benchmark. By filtering out the domain specific evaluation metrics and only considering the evaluation of performance and practical suitability for solving a state space model, the best choice of language was identified.

The study showed that Julia performed significantly better than the other two languages when a numerical solver algorithm was used to solve a policy iterative problem. For example, for a 3^{rd} degree problem, Julia computed the solution within 1.58s compared to 39.30s and 5.07s for Matlab and Python respectively [28]. In order to script the model quickly, readily available packaged systems were required. All languages had a variety of differential equation solvers and optimizers with good documentation. However, Julia had designed its differential equation solver with parameter estimation and sensitivity analysis methods in mind. This meant these packages were easily integrated together.

For the above reasons, Julia was chosen to implement the model. Matlab was also used in the project for providing frequency analysis as it had a readily available package. The performance of the language wasn't considered here since the complexity of the problem was low.

3.2 Data

The network could be used to simulate data recorded by electroencephalogram (EEG) or extracellular recording. Extracellular recording uses an electrode inserted into living tissue to measure electrical activity coming from adjacent cells, usually neurons [29]. Although this is an invasive procedure, it provides a much greater level of precision compared to non-invasive methods. The state space model of the 8-cell network produced data in this form using an 8-d output vector where the membrane potential of each neuron was an output.

EEG is the measurement of electric fields emanating from the brain via electrodes attached to the head. The electric fields are the result of neural signals passing between neurons. When billions of these tiny signals are passed simultaneously in spatially aligned neural populations, the electric fields sum and become strong enough to be measured from outside the head [30]. This measurement technique is preferable for medical professionals since it is non-invasive; however, it is only useful for recording information about large populations of neurons. The state space model of the 8-cell network produced data of this form using a scalar output which was the sum of the AMPA synaptic currents [4] as shown by equation 15.

$$EEG = \frac{1}{N}\sum_{i=1}^{N} i_{AMPA}$$

Equation 15: Modelling EEG data

Data in the form of extracellular recording was used for the parameter estimation problem as it was more practical to implement. This was because each membrane potential was a state variable. The EEG recording was a summation of scaled state variables so the data generated would need to be decoded into the contributions of the individual state variables before the parameter estimation could be performed. EEG data was still used in order to compare the data generated by this state space model with the expected results seen in [4]. This was used to confirm the accuracy of the model.

3.3 Network Implementation

The network was implemented using the *DifferentialEquations* package available in Julia. A mutating function was defined for each type of neuron which returned the respective isolated state space model. These functions were named after the neuron they represented. Another mutating function (*network!*) was defined to collect and connect all the isolated state space models, of the individual neurons, to form one state space model representing the network. This function instantiated all 8 neurons and defined the differential equations for the synaptic currents and synaptic gating variables. By defining the network in this way, the problem parameterised by the network properties effected by Propofol, could be defined following the *Systems of Equations* example provided by the package documentation [31]. This problem definition was then fed as a parameter to the solver.

The *AutoTsit5* algorithm was chosen for the solver since it was a good choice for problems with unknown stiffness [31]. The adaptive auto differentiation was switched off and a constant time step of 2×10^{-4} was used. This ensured the solver provided a solution with suitable resolution and returned a fixed size matrix each time the solver was called. This was important since the solutions under different parameter values were being compared.

Chosen parameter values were assigned to the model dependent on the brain state being represented. These were based on the results of [4]. The parameter values used to model the strong frontal alpha oscillation state were three times larger than the baseline. From this, high-resolution signals were generated over a 5 second time interval. These signals were sampled at a rate of 128 Hz [32] as used by common neural measurement devices. A random noise term was added to represent the background noise picked up by the extracellular recording. Samples from a 64-dimensional Gaussian distribution with zero mean, one variance and zero covariance were added to each sampled data point. Different seeds were used for the noise distribution of the training and test sets to ensure the model was validated on unseen data.

3.3.1 Baseline

The underlying function of the training data was generated using the parameter values set by [4]:

$$\tau_{GABA} = 5.00, \qquad \bar{g}_{\text{GABA\_LTS}} = 0.15, \qquad \bar{g}_{\text{GABA\_RE}} = 0.06$$

The simulated extracellular recordings are illustrated by figure 8. The labelled membrane potential corresponds to each neuron in figure 6. This was the data used for the parameter estimation problem. For the LTS, PY and TC neurons, the pairs produced very similar dynamics; in contrast, the RE neuron pair demonstrated significantly different dynamics. With respect to RE2, a trough was suppressed in the RE1 recording at 1.5s and an additional trough occurred in the RE1 recording at 2.2s.

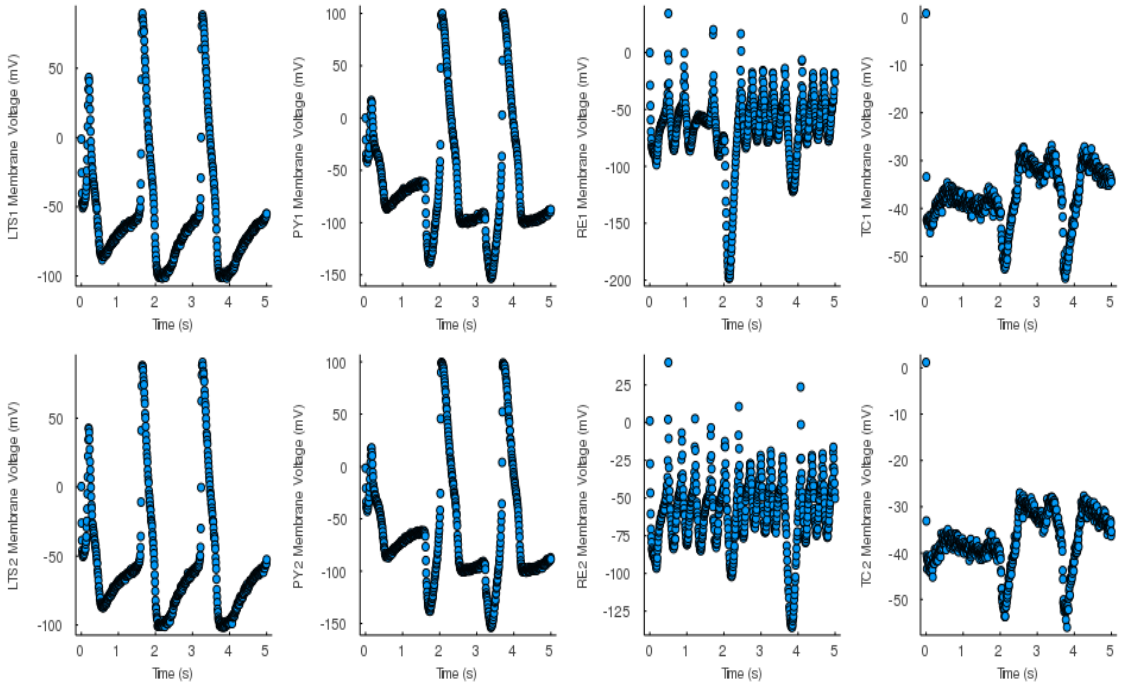

Figure 8: Baseline measured by extracellular recording

The sampled extracellular recording was interpolated and used to compute the EEG reading shown in figure 9. Using the fast Fourier transform, the EEG was analysed in the frequency domain. The power spectral density of the EEG is shown in figure 10. The baseline model had significant frequency components in the 0-12 Hz range and the 25-50 Hz range. This was expected based on the results found in [4] and confirmed the baseline behaviour of the model reproduced realistic data.

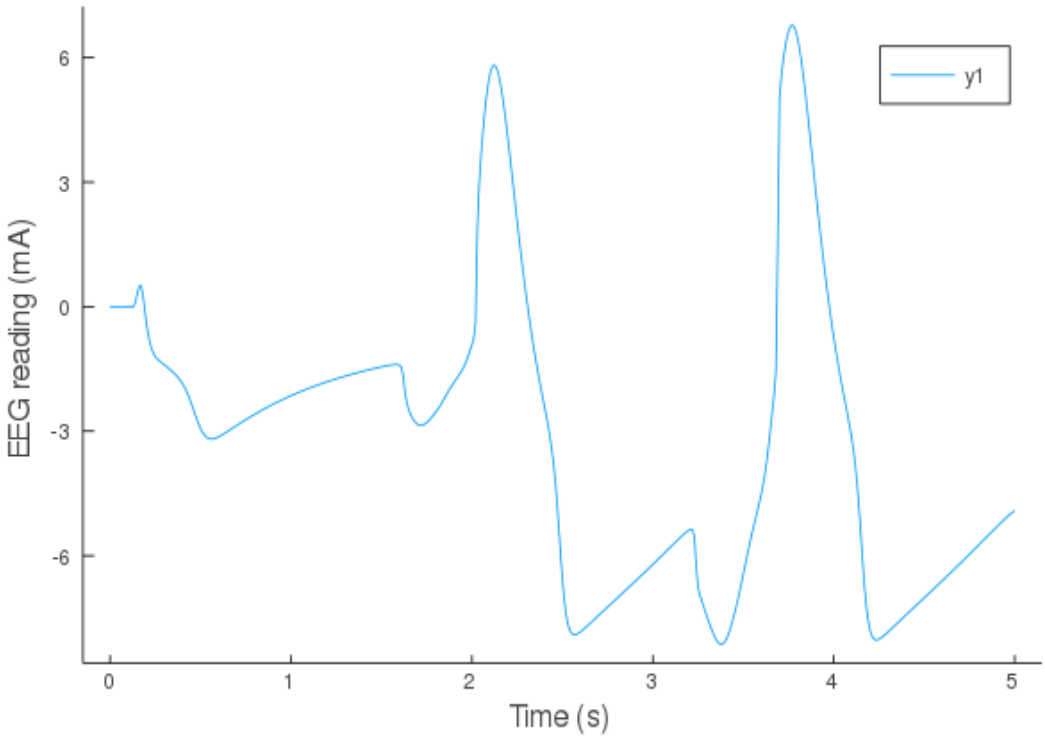

Figure 9: Baseline measured by EEG

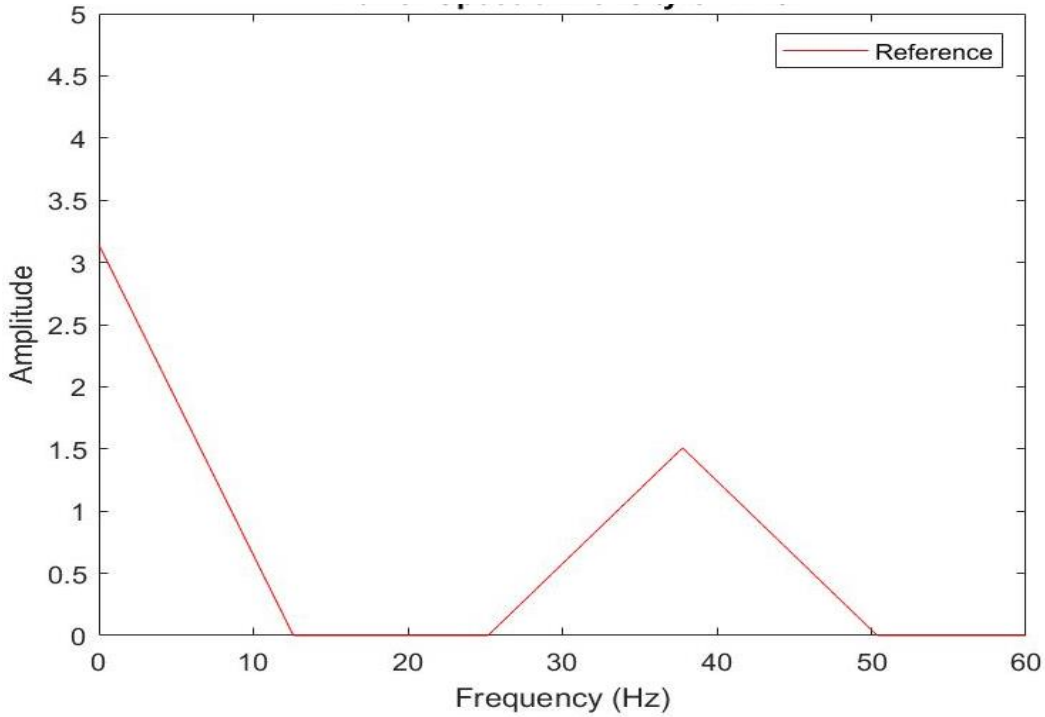

Figure 10: Power spectral density of baseline EEG

3.3.2 Strong Frontal Alpha Oscillation

The training data representing the strong frontal alpha oscillation state was generated by increasing the baseline parameter values by a factor of three [4]:

$$\tau_{GABA} = 15.00, \qquad \bar{g}_{\text{GABA\_LTS}} = 0.45, \qquad \bar{g}_{\text{GABA\_RE}} = 0.18$$

The simulated extracellular recording is illustrated by figure 11. The labelled membrane potential refers to the model shown in figure 6. This was the data used for the parameter estimation problem. Like in the baseline model, the LTS, PY and TC neuron pairs demonstrated very similar dynamics. The RE neuron pair produced differing dynamics; however, the differences weren't as significant as those displayed by the baseline model. In this case, the major troughs occurred at the same time with equal amplitude; but, the periodic components of the waveforms appeared to be different.

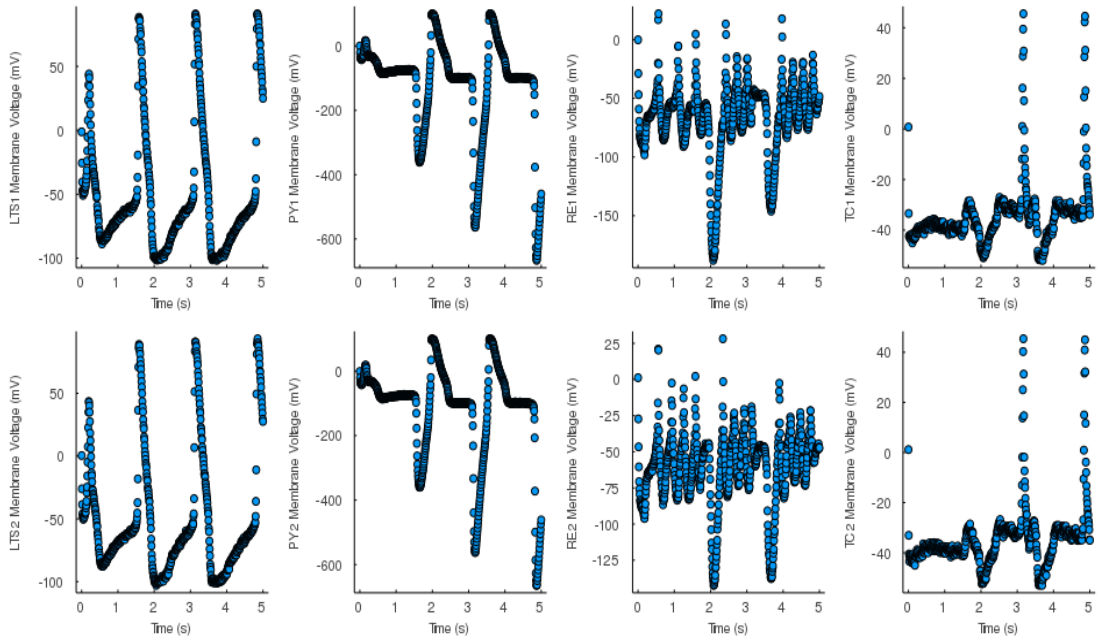

Figure 11: Strong frontal alpha oscillation measured by extracellular recording

With respect to the extracellular recording of the baseline model, this modification to the parameters, caused by the administration of Propofol, triggered the local minimums of the PY1 and PY2 cells to be amplified whereas the local maximums were attenuated. In addition, positive spikes were introduced to the TC1 and TC2 cells at 3s and 5s.

Like before, the extracellular recording was interpolated to compute the continuous EEG shown in figure 12. Again, the fast Fourier transform was used to transform the EEG signal into the frequency domain. The power spectral density of the simulated EEG is shown in figure 13. In comparison to the baseline model, Propofol amplified a local minimum in the EEG at 1.7s from -3mA to -7mA. More significantly, another spike decreased from -8mA to -33mA at 3.3s. Finally, an additional local minimum was introduced at 4.1s where the current stabilised around -8mA before rapidly dropping to -37mA.

The strong frontal alpha oscillation model had significant frequency components in 0-25 Hz, 31-50 Hz and 50-63 Hz ranges. As expected, the power spectral density of the 9-13 Hz range increased significantly due to the increase in parameter values. This was in-line with data observed in [4]. In addition, frequency ranges 12-25 Hz and 50-63 Hz were introduced by this change in parameters whereas the frequency components in the 25-31 Hz range were removed.

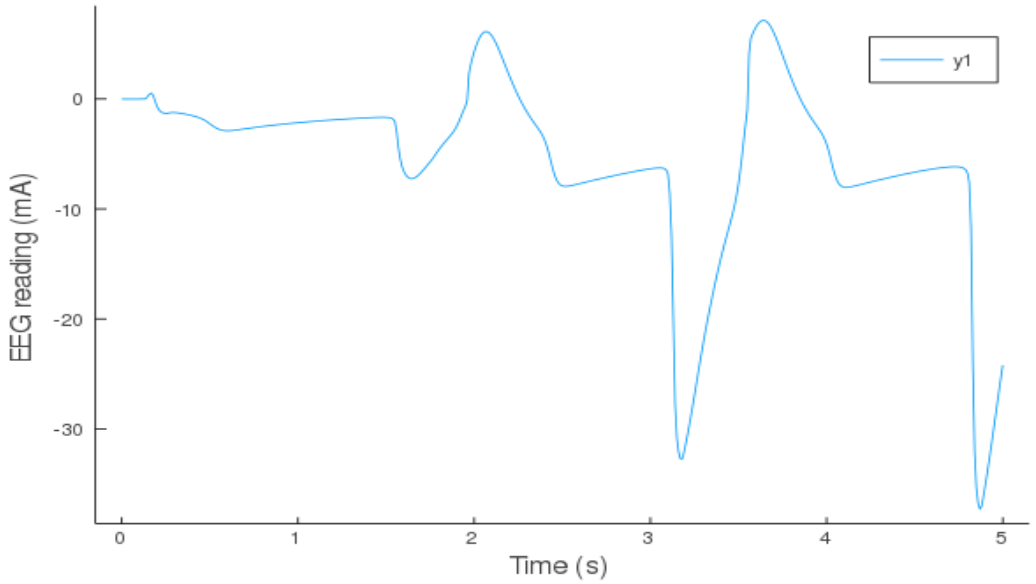

Figure 12: Strong frontal alpha oscillation measured by EEG

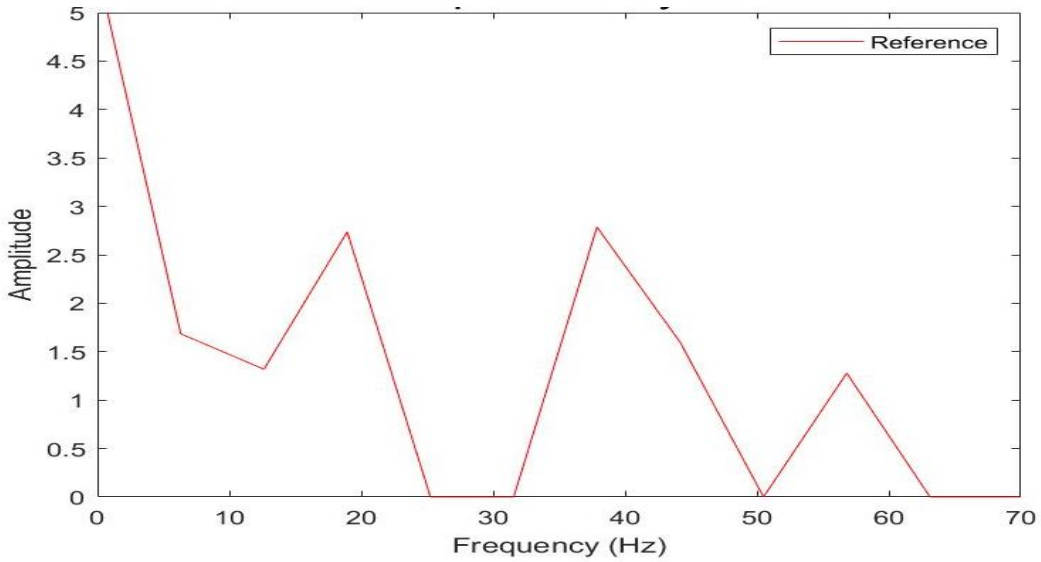

Figure 13: Power spectral density of strong frontal alpha oscillation EEG

Analysis of the EEG confirmed the state space model accurately represented both brain states. In the next section, the model was used to learn the parameter values of the noisy extracellular recordings. These values were used to reproduce clean signals of the recordings. The test data was used to assess how well the estimated parameters modelled the underlying function of the data as opposed to overfitting. These clean signals were then compared to reference signals to determine the brain state.

4 Parameter Estimation

Given the set of noisy membrane potentials measured by the extracellular recording; the aim of this project was to identify the brain state, representing the level of consciousness. As discussed in section 2.4 and demonstrated in section 3.3, the value of the network parameters (GABA time constant, maximal LTS GABA conductance and maximal RE GABA conductance) significantly changed the dynamics of the membrane potentials. The connection between dosage of Propofol and its effect on these parameter values has already been recognised in [4]. Thus, reference signals for each brain state were already established. In this chapter, the process of parameter estimation was explained and demonstrated using case studies of the baseline and strong frontal alpha oscillation brain states. By estimating the parameter values, the inferred models were able to reproduce noise-free signals. The similarity between the inferred model and each reference model was computed. The reference model most similar to the inferred model was identified as the brain state.

4.1 Building an Objective Function

This is a scalar function dependent on the vector of parameters. A similarity measurement was used to map the 3-d input to the scalar output. This measurement evaluated the similarity between the test data matrix and the data matrix generated by the state space model for each vector of parameters in the domain. These matrices were formed of eight columns- each containing the sampled membrane voltage of their respective neuron over a 5s interval. The squared L_2-norm was used as the similarity metric for this objective function and the domain interval was as follows:

$$0.01 \leq \tau_{GABA} \leq 20.00, \qquad 0.01 \leq \bar{g}_{\mathrm{GABA_{LTS}}} \leq 0.60, \qquad 0.01 \leq \bar{g}_{\mathrm{GABA_{RE}}} \leq 0.60$$

Practically, this was implemented using the *DiffEqParamEstim* package. The *build_loss_objective* function was used to build the objective function. The *AutoTsit5* solver was used for repeatedly solving the state space model for each vector of parameters in the domain of the objective function. The *L2Loss* function was used for calculating the squared L_2-norm between the test data matrix and the data matrix corresponding to each vector of parameters- this was the output of the objective function.

4.2 Finding the Optimal Parameter Values

The optimal combination of parameters was the set which minimised the objective function. This set best represented the data measured by the extracellular recording. If the objective function had an analytical description, an optimal point could be found by setting the objective function's gradient equal to zero. The Hessian matrix of the objective function could then be evaluated at the solutions to determine if the respective solution was a maximum, minimum or saddle point. However, since the objective function had no analytical description, a numerical approach was required to find the minimum.

The BFGS algorithm was the chosen optimizer for locating the local minimum. As explained in section 2.7 this algorithm is a local optimization method which required a convergence tolerance to be set. When the magnitude of the objective function's gradient was less than or equal to the convergence tolerance, the algorithm stopped iterating. A parameter vector which mapped to a minimum provided the best fit to the training data in some local region of the parameter space. Other optimizers such as gradient descent were considered however, for ill-conditioned problems, this would be much slower [33]. The use of a global optimisation method was also considered; however, for reasons explained in section 2.8, it was deemed more beneficial to find multiple models which produced similar data to that observed.

The BFGS algorithm was implemented using the *Optim* package. The *optimize* function was used to run the algorithm. The convergence tolerance was set as zero by default, therefore only minimums were found. The optimizer was initiated from twelve equally spread locations in the parameter space. Although there was no way of knowing if the global minimum was found, the probability of the whole parameter space being searched was improved.

4.2.1 Baseline

From the twelve searches, the location of each minimiser was plotted in figure 14. The colour of the data point represents the associated value of the objective function.

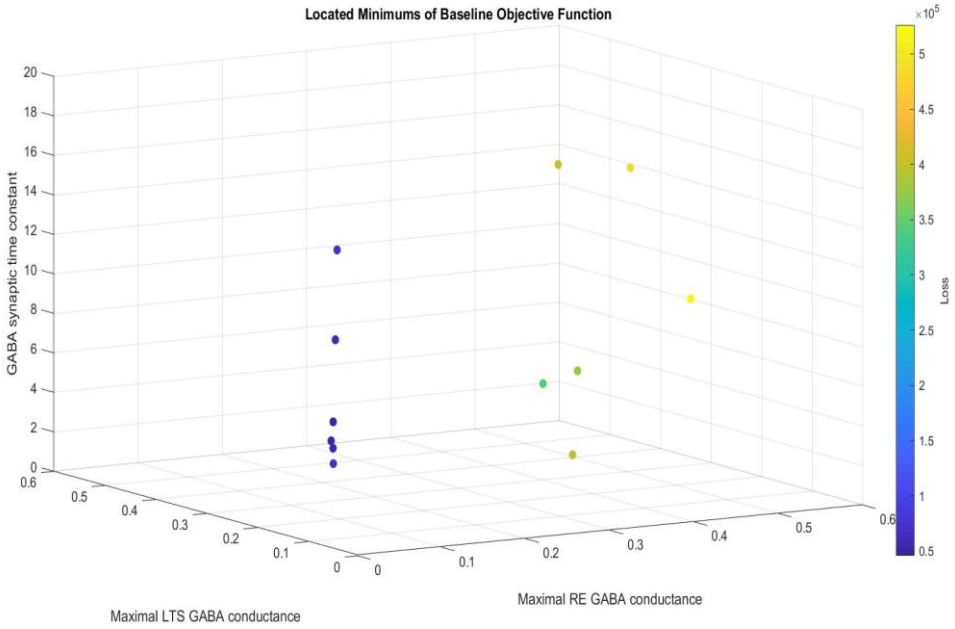

Figure 14: Minimisers of the baseline objective function

The minimisers with the blue dots provided similar representations of the data measured by the extracellular recording. For these six minimisers, the GABA synaptic time constant had a range of 11.140. This was much larger than the range of the maximal GABA conductance's. These were 0.017 and 0.035 for the RE and LTS neuron's respectively. This suggested the network dynamics were far more sensitive to the conductance parameters compared to the time constant. The mean maximal GABA conductance for the RE and LTS neurons were 0.06 and 0.15 respectively. These were the same as the values used for the maximal baseline conductance's; the mean time constant was 6.86 which was 37% larger than the time constant used. This also supported the theory that the network dynamics were less sensitive to the time constant.

The lowest objective function value was 4.58×10^4, this was achieved when the following minimiser was used:

$$\tau_{GABA} = 5.470, \qquad \bar{g}_{\mathrm{GABA\_LTS}} = 0.148, \qquad \bar{g}_{\mathrm{GABA\_RE}} = 0.059$$

Initially, this value seemed very high but when the number of states and the high sampling rate was acknowledged, it was less surprising. The maximal RE and LTS conductance was respectively 2% and 1% smaller than the values used for the underlying function which generated the extracellular recordings. The time constant was 9% larger. Figure 15 shows the solution, generated by the optimal minimiser, plotted on top of the test data. As can be seen, this traced out the test data well for each of the membrane potentials. The squared L_2-norm evaluated the similarity

between each minimiser and the test data. The optimal minimiser generalised best as it had the lowest squared L_2-norm of 204.

Figure 16 shows the solution generated by the optimal minimiser plotted next to the underlying function which produced the extracellular recordings. The optimal solution deviated from the data's underlying function minimally, with the most notable deviations being in the RE1 and RE2 traces.

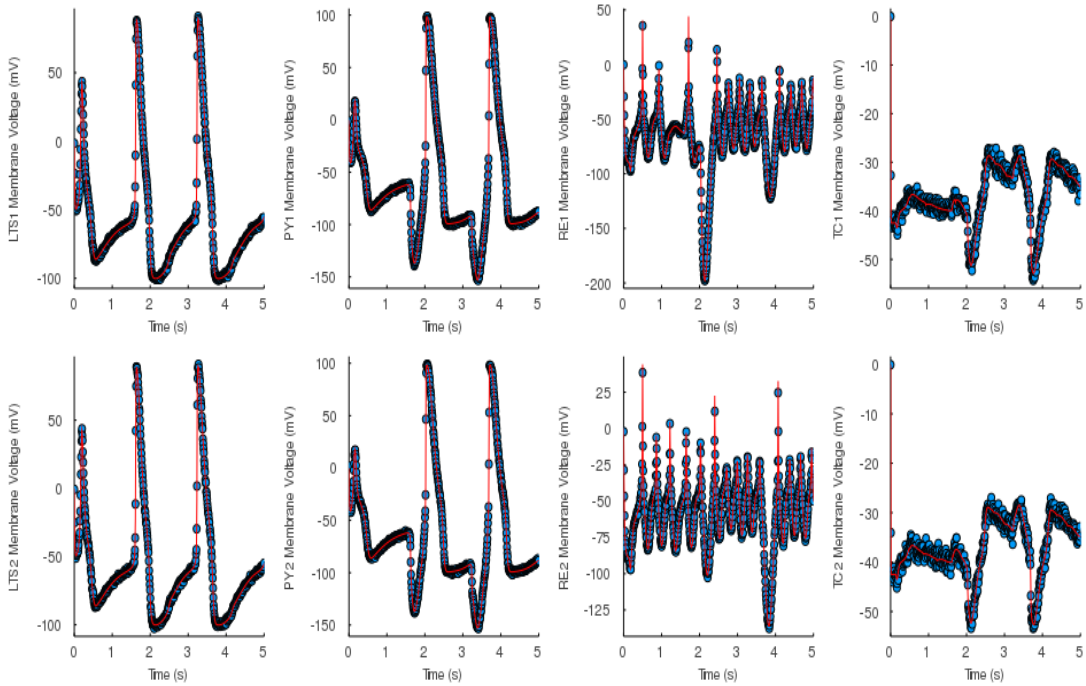

Figure 15: Optimal minimiser baseline model above baseline test data

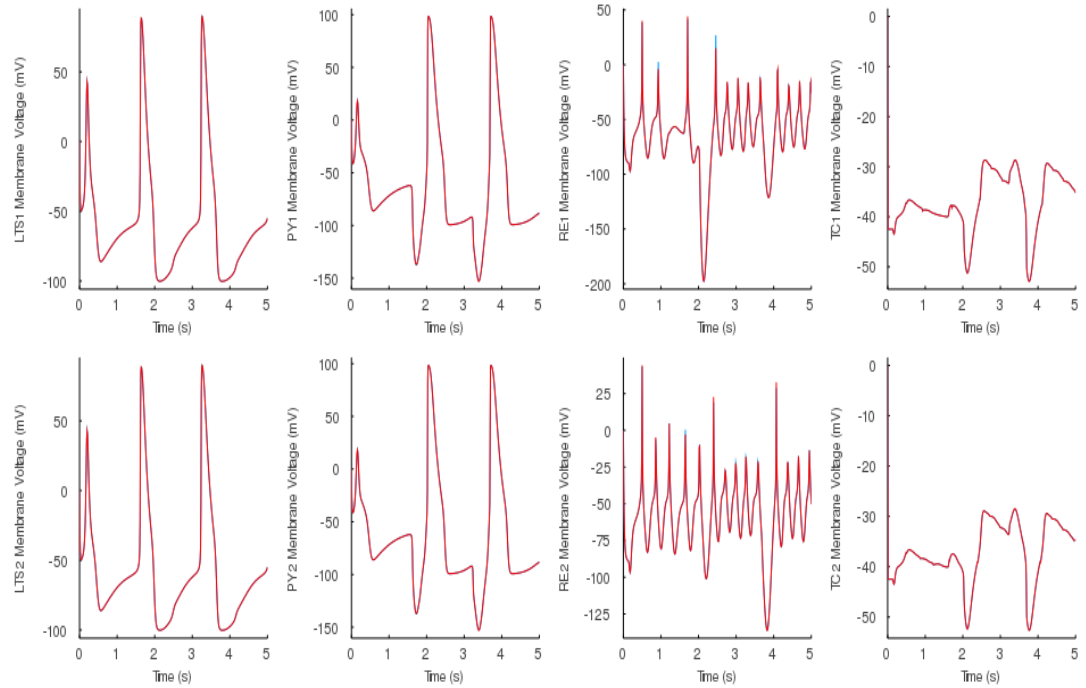

Figure 16: Optimal minimiser baseline model (red) vs underlying model of baseline extracellular recording (blue)

4.2.2 Strong Frontal Alpha Oscillation (SFAO)

From the twelve searches, the location of each minimiser was plotted in figure 17. The colour of the data point represents the associated value of the objective function.

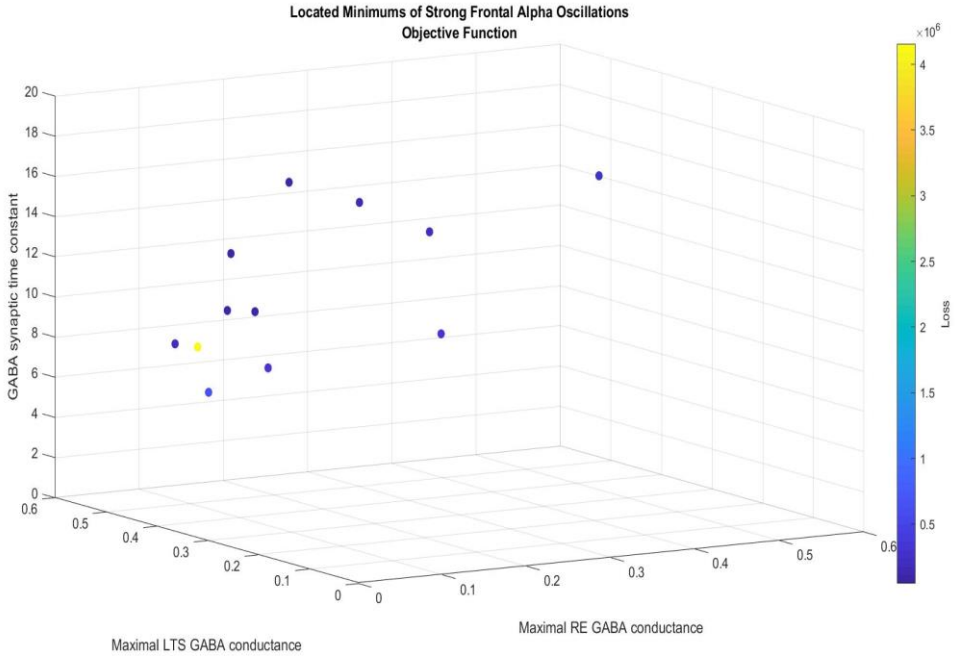

Figure 17: Minimisers of the SFAO objective function

The minimiser with the yellow dot had a much larger loss value than the other results and was treated as an outlier. The data points with the six lowest objective function values were statistically evaluated for comparison with results of the baseline. The range of the GABA synaptic time constant was 6.6, like before, this was a much larger range than the other parameters, although 41% smaller than the respective range of the baseline. The range for the maximal LTS and RE GABA conductance was 0.034 and 0.234 respectively. This suggested the network dynamics of the strong frontal alpha oscillation state were still more sensitive to the maximal conductance values, particularly the LTS, compared to the time constant. The mean maximal LTS and RE conductance values were 0.21 and 0.46 respectively. These were 17% and 2% larger than the parameter values used for the underlying function of the generated data. The mean time constant was 12.5, this was 17% smaller.

The lowest objective function value was 4.95×10^4, this was 8% larger than the lowest baseline. This was achieved when the parameter values were:

$$\tau_{GABA} = 16.000, \qquad \bar{g}_{\mathrm{GABA\_LTS}} = 0.447, \qquad \bar{g}_{\mathrm{GABA\_RE}} = 0.186$$

The maximal LTS and RE conductance was 1% smaller and 3% larger than the values used for the underlying function which generated the extracellular recordings. The time constant was 7% larger. Figure 18 shows the solution, produced by the optimal minimiser, plotted above the test data. This traced out the test data well for each membrane potential. This solution produced the best similarity score, calculated by the squared L_2-norm, when measured against the test data- the score was 206. Figure 19

shows the solution generated by the optimal minimiser plotted next to the underlying function which produced the test data. The only visible deviations occurred on the RE1 and RE2 traces, but these were minimal.

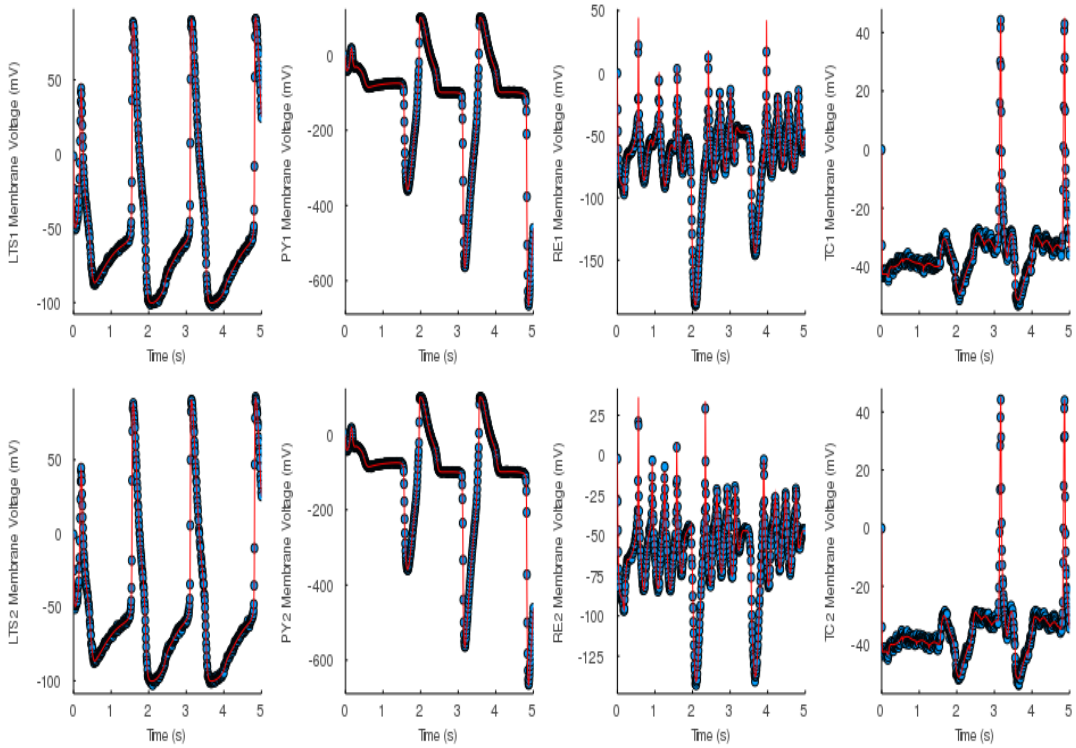

Figure 18: Optimal minimiser SFAO model above SFAO test data

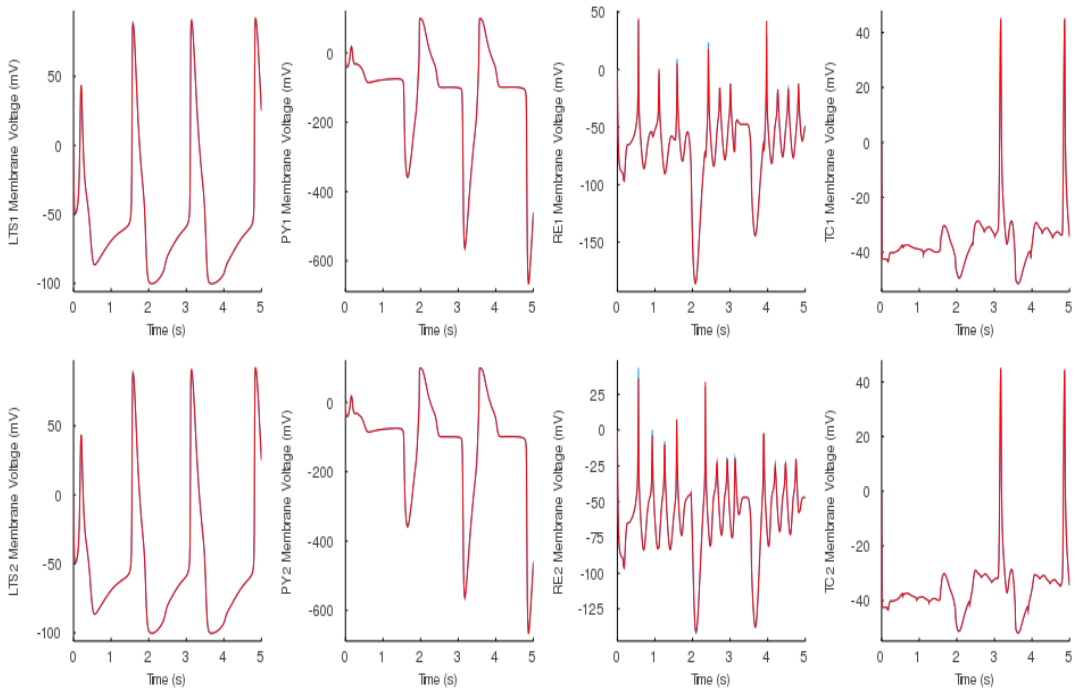

Figure 19: Optimal minimiser SFAO model (red) vs underlying model of SFAO extracellular recording (blue)

4.3 Choosing a Brain State

Once a model of the extracellular recording was inferred, a decision had to be made as to what brain state it was. To do this, the L_2-norm measured the similarity between the inferred model and the reference models of the baseline and strong frontal alpha oscillation brain states. The brain state which minimised the L_2-norm was chosen. Equation 16 shows the decision function where R_i represents the reference matrix and M represents the inferred matrix of the 8 membrane voltages.

$$f(R_i) = \begin{cases} 1, & if \min\left|\left|R_i - M\right|\right|_2^2 \; where \; i = baseline \\ 0, & if \min\left|\left|R_i - M\right|\right|_2^2 \; where \; i = strong \; frontal \end{cases}$$

Equation 16: Decision function

The reference matrices, of each brain state, were formed by the respective parameter values that generated the underlying function of the data in section 3.3.1 and 3.3.2. Figure 20 shows the inferred baseline model plotted against the baseline reference and figure 21 shows the inferred baseline model plotted against the strong frontal alpha oscillation reference.

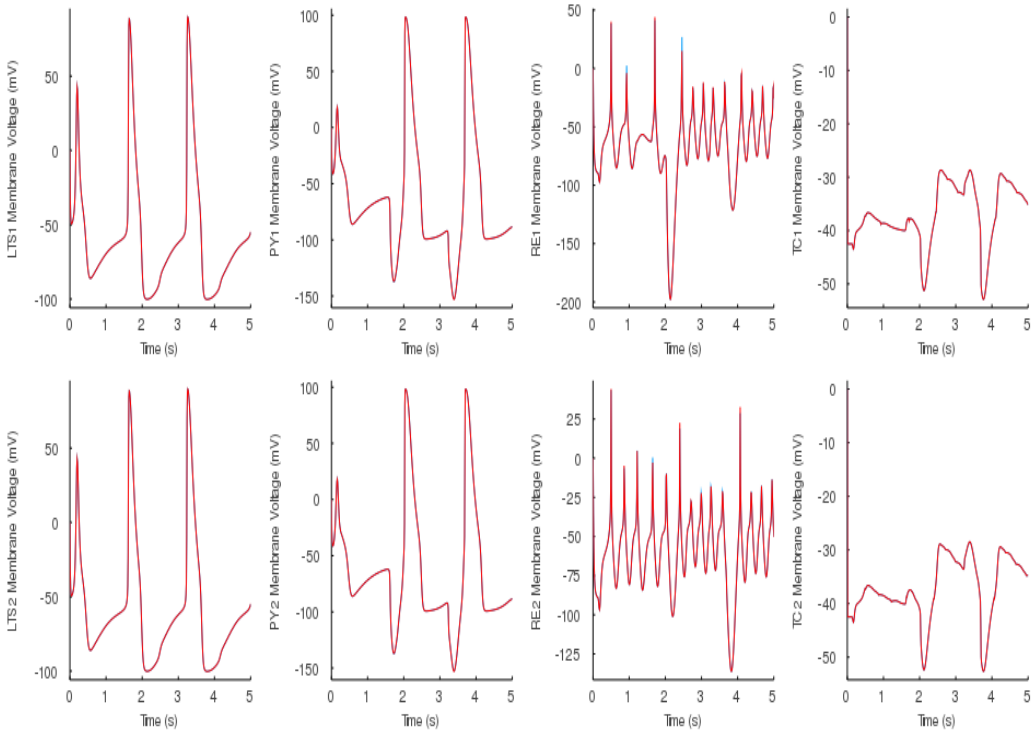

Figure 20: Inferred baseline model (red) vs baseline reference (blue)

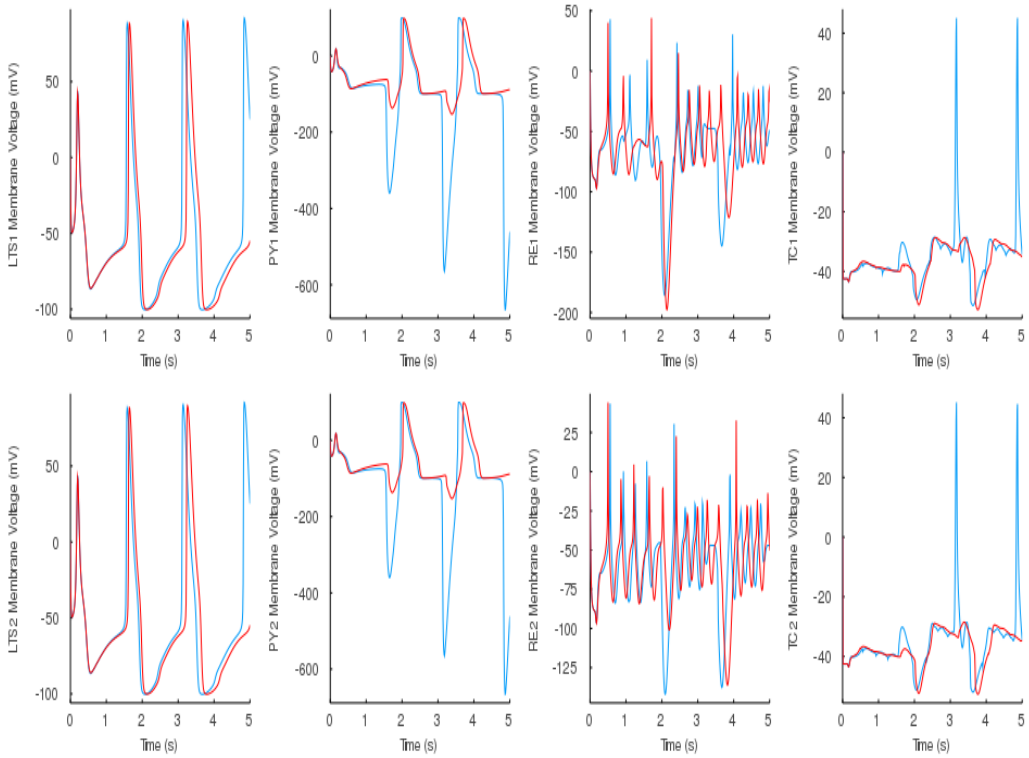

Figure 21: Inferred baseline model (red) vs SFAO reference (blue)

Figure 22 shows the inferred strong frontal alpha oscillation model plotted against the baseline reference and figure 23 shows the inferred strong frontal alpha oscillation model plotted against the strong frontal alpha oscillation reference.

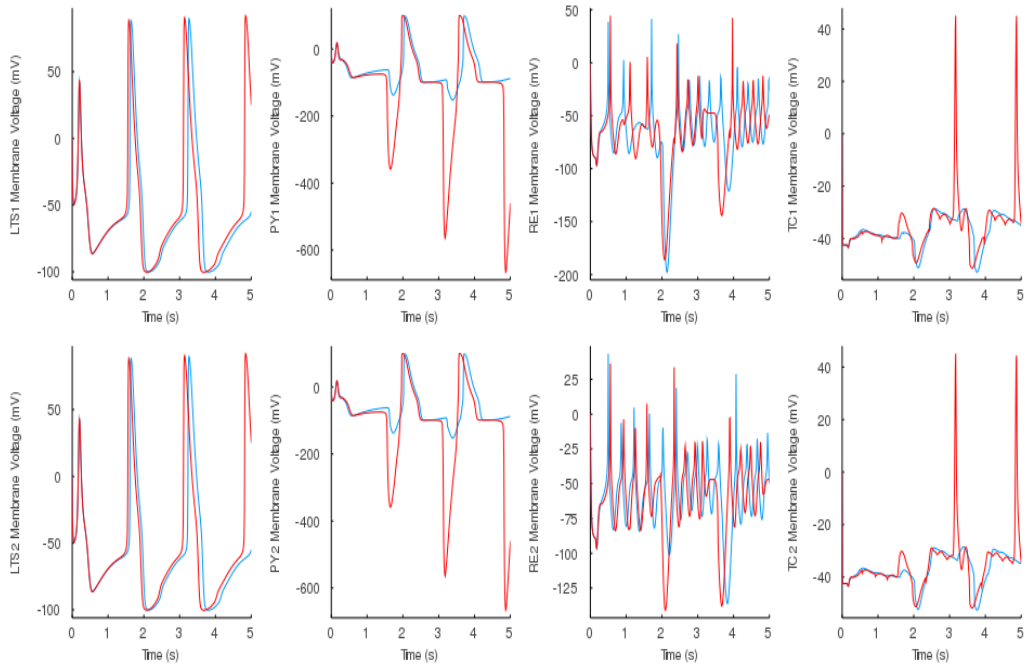

Figure 22: Inferred SFAO model (red) vs baseline reference (blue)

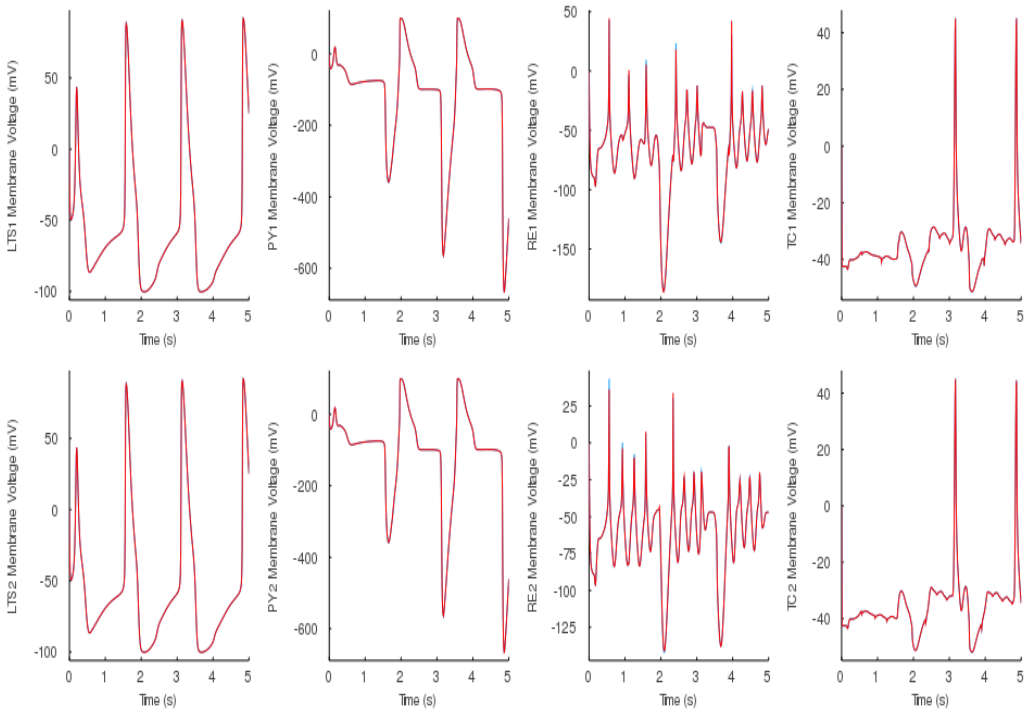

Figure 23: Inferred SFAO model (red) vs SFAO reference (blue)

The calculated L_2-norms between each optimal inferred model and each reference model are shown in table 1. As can be seen from table 1, the decision function chose the correct brain state for each inferred model. Under normal conditions, the brain state of the inferred model would be unknown until the result of the decision function was obtained.

Inferred model, M	**Reference model, R_i**	**L_2-Norm**
baseline	i = baseline	204
baseline	i = strong frontal alpha oscillation	5211
Strong frontal alpha oscillation	i = baseline	5212
Strong frontal alpha oscillation	i = strong frontal alpha oscillation	206

Table 1: Decision functions results

Results from sections 4.2.1 and 4.2.2 showed that, for both brain states, several models were estimated which produced network dynamics like the respective underlying dynamics of the extracellular recordings. As explained in section 2.8, this indicated the deviation between the estimated and true parameter values, of these models, were compensated for. Results from section 4.3 show the correct brain state was chosen for each case study.

5 Sensitivity Analysis

The previous chapter used an optimisation method to identify a set of models which minimised an objective function. The model which best represented the noisy extracellular recordings was then established. These models were parameterised by the maximal GABA conductance and decay time which controlled the dynamics of the network, based on the level of Propofol present. These parameter values were used to identify the brain state which represented the level of consciousness. This chapter investigated the stability of each case study's optimal model. It considered the sensitivity of each membrane potential to each network parameter and demonstrated, across the time series, where the small perturbations would significantly affect the dynamics produced by that model.

To conduct the sensitivity analysis, the *DiffEqSensitivity* package was used. The problem was setup following the *ODELocalSensitivityProblem* section of the documentation [34]. For each model, the *AutoTsit5* algorithm computed the sensitivity of each state to each parameter.

5.1 Baseline

The sensitivity of each membrane potential to the GABA time constant was plotted next to their corresponding membrane potential in figure 24. It shows each membrane potential was relatively insensitive, across the time series, to the GABA time constant. This was predicted in section 4.2.1; some located minimisers had large deviations from the true GABA time constant, but the deviation of the conductance was always much smaller. The spikes in the sensitivity to this parameter occurred mostly at the beginning of large peaks in the corresponding membrane potential and occasionally at the beginning of large troughs.

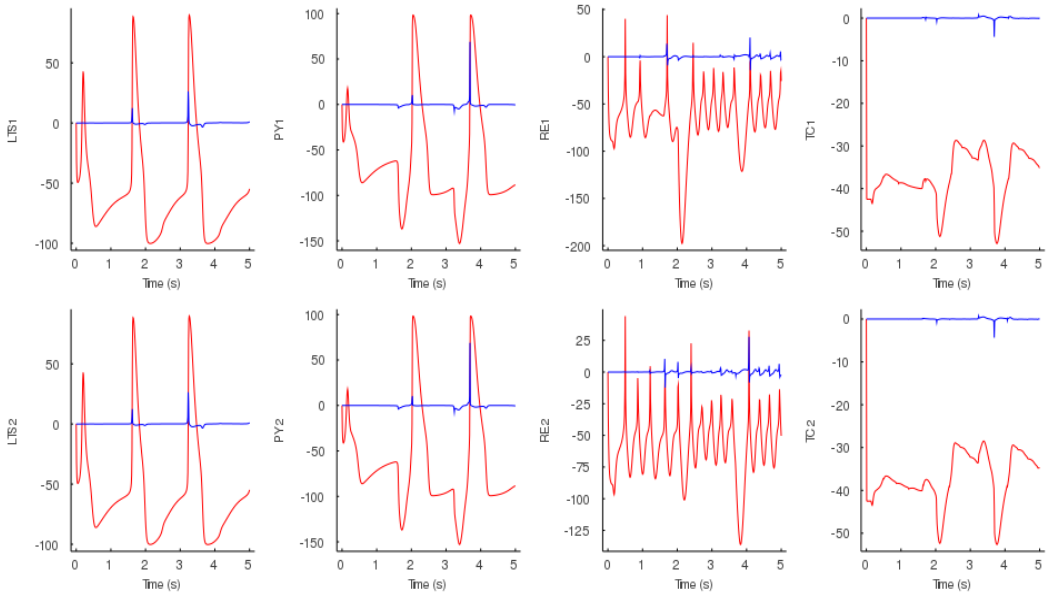

Figure 24: Inferred baseline membrane potentials (red) and their sensitivity to GABA time constant (blue)

Figure 25 shows, for large portions of the time series, each cortical membrane potential was relatively insensitive to the maximal LTS GABA conductance. However, each potential had one very large peak and an additional smaller peak. The RE cells, located in the thalamus, were sensitive across the time series. The TC cells were relatively insensitive to this parameter, but each displayed a large trough at 3.8s.

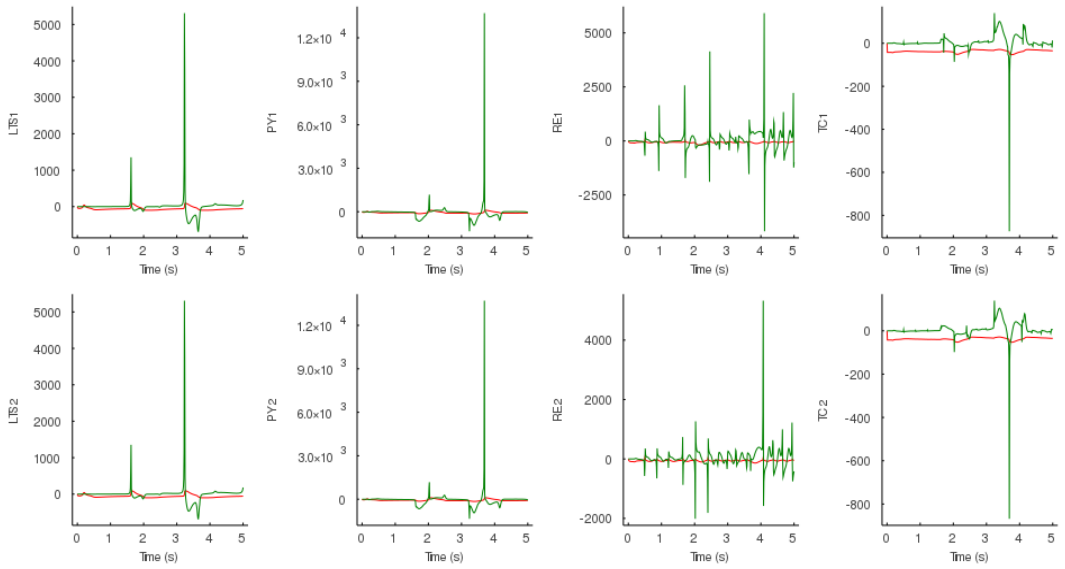

Figure 25: Inferred baseline membrane potentials (red) and their sensitivity to maximal LTS GABA conductance (green)

Figure 26 shows each of the cortical membrane potentials were perfectly insensitive, across the full time series, to the maximal RE GABA conductance. Both TC cells were relatively insensitive across the time series; whereas, the differing dynamics of the RE neuron pair produced varying sensitivity behaviour. The sensitive behaviour of RE2 was focused around one large spike at 2s. On the other hand, RE1 had three large spikes throughout the time series.

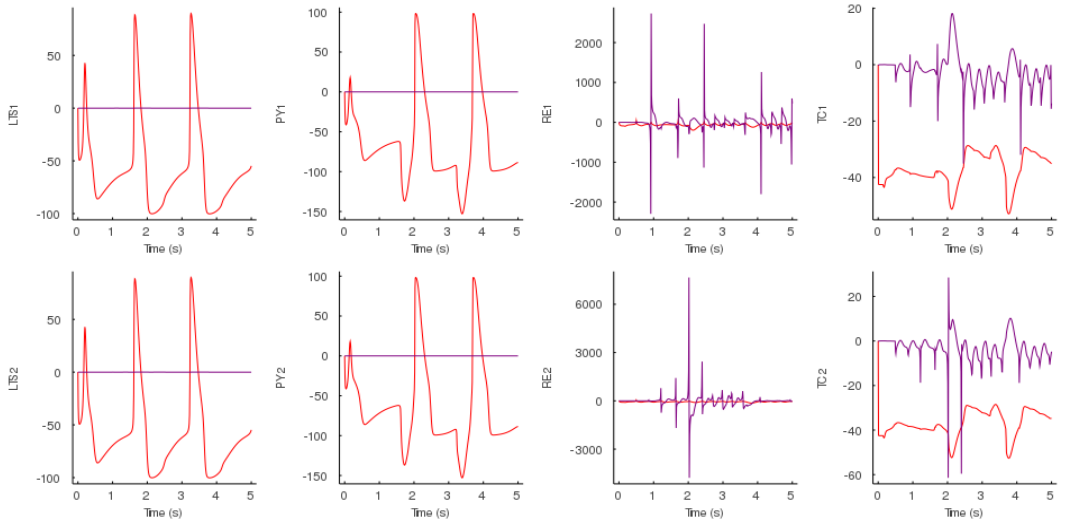

Figure 26: Inferred baseline membrane potentials (red) and their sensitivity to maximal RE GABA conductance (purple)

5.2 Strong Frontal Alpha Oscillation (SFAO)

Figure 27 shows the dynamics of the model, in the strong frontal alpha oscillation brain state, were robust to a change in the GABA time constant across the time series. This was predicted in section 4.2.2 since the range of time constant values, across the minimisers, was much larger than the conductance parameters.

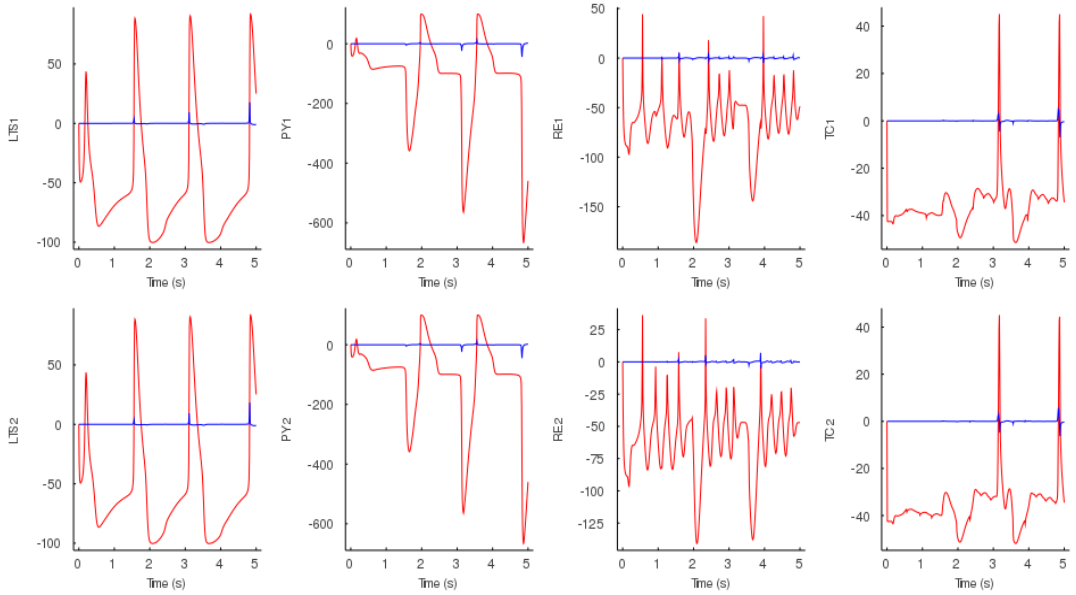

Figure 27: Inferred SFAO membrane potentials (red) and their sensitivity to GABA time constant (blue)

Figure 28 shows the LTS neurons had three large peaks in their sensitivity to maximal LTS GABA conductance and the PY cells had two large troughs. Like in the baseline model, the RE1 and RE2 neurons were sensitive to the maximal LTS GABA conductance throughout the time series; whereas, the TC cells were insensitive across the time series apart from two large spikes.

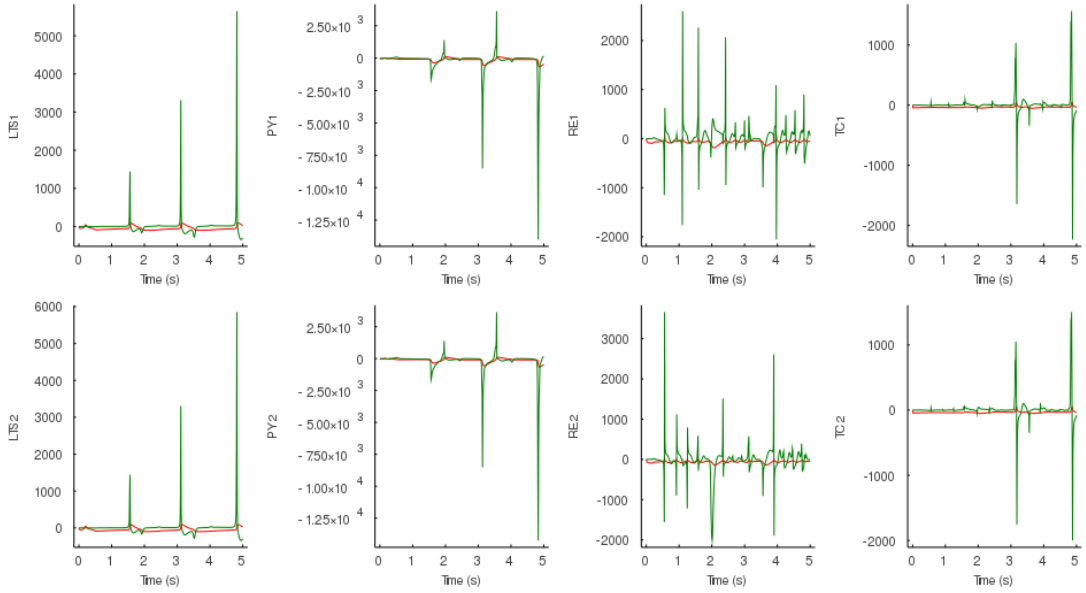

Figure 28: Inferred SFAO membrane potentials (red) and their sensitivity to maximal LTS GABA conductance (green)

Figure 29 demonstrates the increased dosage of Propofol did not change the sensitivity, of the cortical neurons, to the maximal RE GABA conductance. They remained insensitive across the time series. The TC neurons were also relatively insensitive across the time series. RE1 had a large spike at 2s and 4s whereas RE2 had only one large spike at 2s.

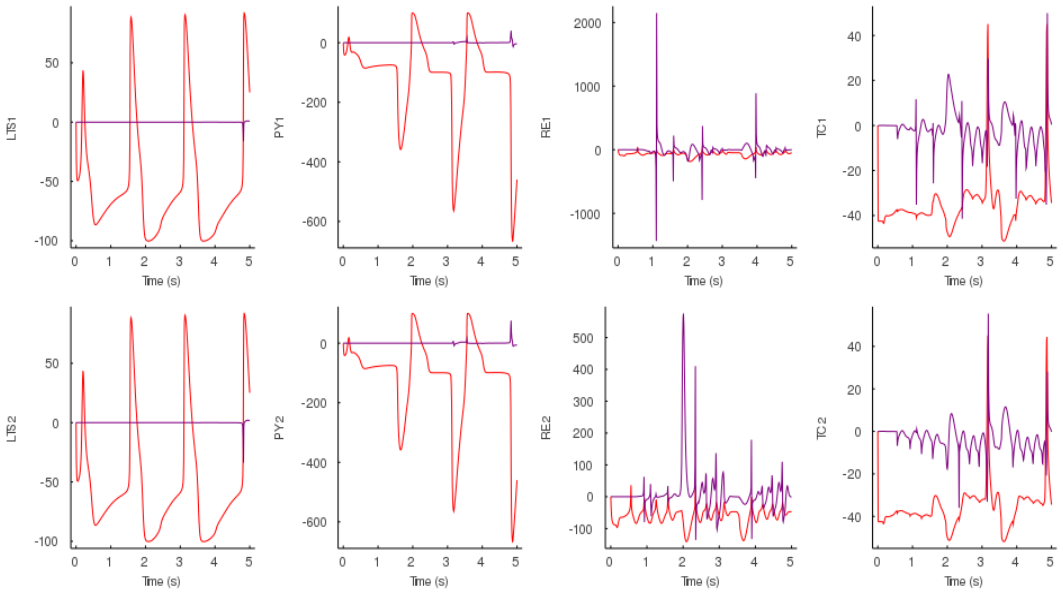

Figure 29: Inferred SFAO membrane potentials (red) and their sensitivity to maximal RE GABA conductance (purple)

To summarise, the optimal baseline model was insensitive to the GABA time constant across all neurons. The cortical neurons were very sensitive to the maximal LTS GABA conductance for short periods of the time series. The neurons located in the thalamus were all sensitive, across the time series, to the maximal LTS and RE GABA conductance's. The optimal strong frontal alpha oscillation model was insensitive to the GABA time constant. The cortical neurons were very sensitive to the LTS GABA conductance; whereas the neurons located in the thalamus were sensitive to both conductance's, particularly, the LTS GABA conductance.

6 Conclusion

The results of the parameter estimation demonstrated the local optimisation method succeeded in finding a group of models that replicated the underlying dynamics of the noisy extracellular recordings. Although none of the models were identical to those used to generate the observed recordings, this did not matter. If this was the case, a global optimisation method would have been used. Finding a collection of models which approximated the recordings well was more representative of a biological network [7]. Since the models represented the dynamics of the recordings well, the correct brain state, representing the level of consciousness, was identified. This was demonstrated using the optimal set of parameters for each brain state. Thus, the aim of the project was achieved. The sensitivity analysis also supported the prediction that the models were much more sensitive to perturbations in the conductance values compared to the time constant.

The next step in this line of research would be to extend the number of brain states, representing various levels of consciousness, being considered to include paradoxical excitation, anteriorization and burst suppression. If this works, the same procedure could be considered for non-invasive measurements, like EEG recordings. This would require state estimation methods, like Kalman filtering, to approximate the time series of the membrane potentials. If this could be done accurately, the procedure outlined in this research could be used to estimate the model parameters and then identify the correct brain state.

7 Project Management

This multi-disciplinary project involved a lot of background research since the biological concepts of this model were not well understood, initially. Due to this limited understanding, the initial project plan was regularly reviewed throughout the project. This was demonstrated by the difference between the initial and executed project plans shown in appendix B. At the beginning of the project, it was decided that, the report should be written after the work had been completed. It was felt there would be a clearer narrative for the report at this stage. The first semester was primarily focused on implementing the model. This was done incrementally, first by modelling the individual neurons and then by incorporating them into the network. The original target was to complete this before the Christmas break; however, difficulties occurred when trying to form the network which forced this too take longer than planned. This was the extend of the delays suffered. The second semester was focused on the machine learning aspect of the project. This was better understood, so less time was needed. Many challenges were faced during the second semester due to COVID-19; however, the length of time taken to complete the project was scaled proportionally to the extension given. No other issues occurred which was testament to the success of the risk assessment, shown in appendix C.

Main body word count: 8,337

References

[1] S. Herculano-Houzel, "The human brain in numbers: a linearly scaled-up primate brain," (in English), *Frontiers in Human Neuroscience,* Review vol. 3, no. 31, 2009-November-09 2009, doi: 10.3389/neuro.09.031.2009.

[2] D. A. Drachman, "Do we have brain to spare?," *Neurology,* vol. 64, no. 12, pp. 2004-2005, 2005, doi: 10.1212/01.Wnl.0000166914.38327.Bb.

[3] P. Alcami, R. Franconville, I. Llano, and A. Marty, "Measuring the Firing Rate of High-Resistance Neurons with Cell-Attached Recording," *The Journal of Neuroscience,* vol. 32, no. 9, pp. 3118-3130, 2012, doi: 10.1523/jneurosci.5371-11.2012.

[4] S. Ching, A. Cimenser, P. L. Purdon, E. N. Brown, and N. J. Kopell, "Thalamocortical model for a Propofol-induced α-rhythm associated with loss of consciousness," *Proceedings of the National Academy of Sciences,* vol. 107, no. 52, p. 22665, 2010, doi: 10.1073/pnas.1017069108.

[5] A. L. Hodgkin and A. F. Huxley, "A quantitative description of membrane current and its application to conduction and excitation in nerve," *The Journal of physiology,* vol. 117, no. 4, pp. 500-544, 1952.

[6] P. Hagmann, "The brain represented as a network," ed. CHUV-UNIL, Lausanne, Switzerland: MR connectomics.

[7] E. Marder and A. L. Taylor, "Multiple models to capture the variability in biological neurons and networks," *Nature Neuroscience,* vol. 14, no. 2, pp. 133-138, 2011/02/01 2011, doi: 10.1038/nn.2735.

[8] K. J. Aström, R. M. Murray, and K. J. Astr M, *Feedback Systems : An Introduction for Scientists and Engineers*. New Jersey, UNITED STATES: Princeton University Press, 2010.

[9] P. Dayan and L. F. Abbott, *Theoretical neuroscience*. Cambridge, MA: MIT Press, 2001.

[10] M. M. McCarthy, E. N. Brown, and N. Kopell, "Potential Network Mechanisms Mediating Electroencephalographic Beta Rhythm Changes during Propofol-Induced Paradoxical Excitation," *The Journal of Neuroscience,* vol. 28, no. 50, pp. 13488-13504, 2008, doi: 10.1523/jneurosci.3536-08.2008.

[11] D. Silverthorn, *Human Physiology: An Integrated Approach*. Harlow: Pearson Education, 2016.

[12] X.Zhu. "Toward brain-like computing: New memristor better mimics synapses." Nanoelectronics Group, University of Michigan. https://news.umich.edu/toward-brain-like-computing-new-memristor-better-mimics-synapses/ (accessed 3, December, 2019).

[13] S. Ching and E. N. Brown, "Modeling the dynamical effects of anesthesia on brain circuits," *Current Opinion in Neurobiology,* vol. 25, pp. 116-122, 2014/04/01/ 2014, doi: https://doi.org/10.1016/j.conb.2013.12.011.

[14] J. B. D. Gommers, "Medications for analgesia and sedation in the intensive care unit: an overview," *Crit Care,* vol. 12, no. S4, 3, 2008.

[15] D. Bai, P. S. Pennefather, J. F. MacDonald, and B. A. Orser, "The general anesthetic Propofol slows deactivation and desensitization of GABA(A) receptors," *Journal of Neuroscience,* Article vol. 19, no. 24, pp. 10635-10646, 1999.

[16] F. F. E. Brown. (2019) General Anesthesia Causes Telltale Brain Activity Patterns. *The Scientist*.
[17] S. A. Fulton and K. D. Mullen, "Completion of upper endoscopic procedures despite paradoxical reaction to midazolam: A role for flumazenil?," *American Journal of Gastroenterology,* Article vol. 95, no. 3, pp. 809-811, 2000, doi: 10.1016/S0002-9270(99)00925-9.
[18] L. D. Gugino, R. J. Chabot, L. S. Prichep, E. R. John, V. Formanek, and L. S. Aglio, "Quantitative EEG changes associated with loss and return of consciousness in healthy adult volunteers anaesthetized with Propofol or sevoflurane," *British Journal of Anaesthesia,* Article vol. 87, no. 3, pp. 421-428, 2001, doi: 10.1093/bja/87.3.421.
[19] E. N. Brown, R. Lydic, and N. D. Schiff, "General anesthesia, sleep, and coma," *New England Journal of Medicine,* Review vol. 363, no. 27, pp. 2638-2650, 2010, doi: 10.1056/NEJMra0808281.
[20] A. Cimenser *et al.*, "Tracking brain states under general anesthesia by using global coherence analysis," *Proceedings of the National Academy of Sciences of the United States of America,* Article vol. 108, no. 21, pp. 8832-8837, 2011, doi: 10.1073/pnas.1017041108.
[21] V. A. Feshchenko, R. A. Veselis, and R. A. Reinsel, "Propofol-induced alpha rhythm," *Neuropsychobiology,* Article vol. 50, no. 3, pp. 257-266, 2004, doi: 10.1159/000079981.
[22] P. L. Purdon *et al.*, "Electroencephalogram signatures of loss and recovery of consciousness from Propofol," *Proceedings of the National Academy of Sciences of the United States of America,* Article vol. 110, no. 12, pp. E1142-E1151, 2013, doi: 10.1073/pnas.1221180110.
[23] A. Lüthi and D. A. McCormick, "H-current: properties of a neuronal and network pacemaker," *Neuron,* vol. 21, no. 1, pp. 9-12, 1998.
[24] X. Ma, Q. Ye, and H. Yan, "L2P-Norm Distance Twin Support Vector Machine," *IEEE Access,* vol. 5, pp. 23473-23483, 2017, doi: 10.1109/ACCESS.2017.2761125.
[25] S. J. W. Jorge Nocedal, *Numerical Optimization*. New York: Springer, 2006.
[26] A. L. Taylor, T. J. Hickey, A. A. Prinz, and E. Marder, "Structure and Visualization of High-Dimensional Conductance Spaces," *Journal of Neurophysiology,* vol. 96, no. 2, pp. 891-905, 2006, doi: 10.1152/jn.00367.2006.
[27] A. A. Prinz, D. Bucher, and E. Marder, "Similar network activity from disparate circuit parameters," *Nature Neuroscience,* vol. 7, no. 12, pp. 1345-1352, 2004/12/01 2004, doi: 10.1038/nn1352.
[28] C. Coleman, S. Lyon, L. Maliar, and S. Maliar, "Matlab, Python, Julia: What to Choose in Economics?," 2018.
[29] P. Fromherz, "Extracellular recording with transistors and the distribution of ionic conductances in a cell membrane," *European Biophysics Journal,* vol. 28, no. 3, pp. 254-258, 1999.
[30] M. X. Cohen, "Where does EEG come from and what does it mean?," *Trends in neurosciences,* vol. 40, no. 4, pp. 208-218, 2017.
[31] *DifferentialEquations.jl*. (2016). Accessed: 22/04/2020. [Online]. Available: https://docs.sciml.ai/stable/
[32] G. Antoniol and P. Tonella, "EEG data compression techniques," *IEEE Transactions on Biomedical Engineering,* vol. 44, no. 2, pp. 105-114, 1997, doi: 10.1109/10.552239.

[33] *Optim.jl*. (2012). [Online]. Available: https://julianlsolvers.github.io/Optim.jl/stable/#
[34] *DiffEqSensitivty.jl*. (2016). [Online]. Available: https://docs.sciml.ai/stable/analysis/sensitivity/

Appendix A- Data

Initial P = [Tau, g_GABA_L, g_GABA_R]	Minimizer P	Value of objective function	L2-norm between model and test data
[5.0, 0.2, 0.2]	[3.16e+00, 1.68e-01, 7.21e-02]	7.14E+04	2.50E+02
[5.0, 0.2, 0.4]	[2.07e+00, 2.01e-01, 3.76e-01]	3.96E+05	6.20E+02
[5.0, 0.4, 0.2]	[4.46e+00, 1.54e-01, 6.11e-02]	4.72E+04	2.07E+02
[5.0, 0.4, 0.4]	[4.02e+00, 1.60e-01, 6.70e-02]	5.41E+04	2.23E+02
[10.0, 0.2, 0.2]	[5.47e+00, 1.48e-01, 5.99e-02]	4.58E+04	2.05E+02
[10.0, 0.2, 0.4]	[6.86e+00, 1.43e-01, 3.47e-01]	3.81E+05	6.08E+02
[10.0, 0.4, 0.2]	[9.73e+00, 1.36e-01, 5.53e-02]	5.76E+04	2.34E+02
[10.0, 0.4, 0.4]	[1.00e+01, 1.36e-01, 4.77e-01]	5.26E+05	7.20E+02
[15.0, 0.2, 0.2]	[1.75e+01, 1.33e-01, 3.18e-01]	4.03E+05	6.23E+02
[15.0, 0.2, 0.4]	[6.39e+00, 1.43e-01, 3.06e-01]	3.39E+05	5.76E+02
[15.0, 0.4, 0.2]	[1.43e+01, 1.33e-01, 5.56e-02]	6.85E+04	2.56E+02
[15.0, 0.4, 0.4]	[1.70e+01, 1.30e-01, 4.02e-01]	4.84E+05	6.85E+02

Table 2: Optimising baseline objective function

Initial P = [Tau, g_GABA_L, g_GABA_R]	Minimizer P	Value of objective function	L2-norm between model and test data
[10.0, 0.4, 0.4]	[4.75e+00, 5.71e-01, 1.65e-01]	6.56E+05	8.08E+02
[5.0, 0.2, 0.4]	[6.01e+00, 5.35e-01, 2.14e-01]	3.59E+05	5.93E+02
[15.0, 0.2, 0.2]	[7.06e+00, 5.71e-01, 1.52e-01]	4.15E+06	2.02E+03
[15.0, 0.2, 0.4]	[7.06e+00, 5.11e-01, 4.05e-01]	3.07E+05	5.38E+02
[15.0, 0.4, 0.4]	[1.47e+01, 4.52e-01, 5.57e-01]	2.91E+05	5.33E+02
[5.0, 0.2, 0.2]	[9.40e+00, 4.81e-01, 1.66e-01]	9.93E+04	3.09E+02
[15.0, 0.4, 0.2]	[1.46e+01, 4.51e-01, 2.72e-01]	1.51E+05	3.75E+02
[5.0, 0.4, 0.4]	[1.27e+01, 4.59e-01, 3.60e-01]	1.79E+05	4.08E+02
[10.0, 0.4, 0.2]	[1.26e+01, 4.62e-01, 1.26e-01]	8.17E+04	2.65E+02
[10.0, 0.2, 0.4]	[1.60e+01, 4.47e-01, 1.86e-01]	4.95E+04	2.05E+02
[10.0, 0.2, 0.2]	[8.09e+00, 4.93e-01, 7.83e-02]	2.12E+05	4.47E+02
[5.0, 0.4, 0.2]	[9.62e+00, 4.79e-01, 1.32e-01]	1.04E+05	3.13E+02

Table 3: Optimising strong frontal alpha oscillations objective function

Appendix B- Project Management

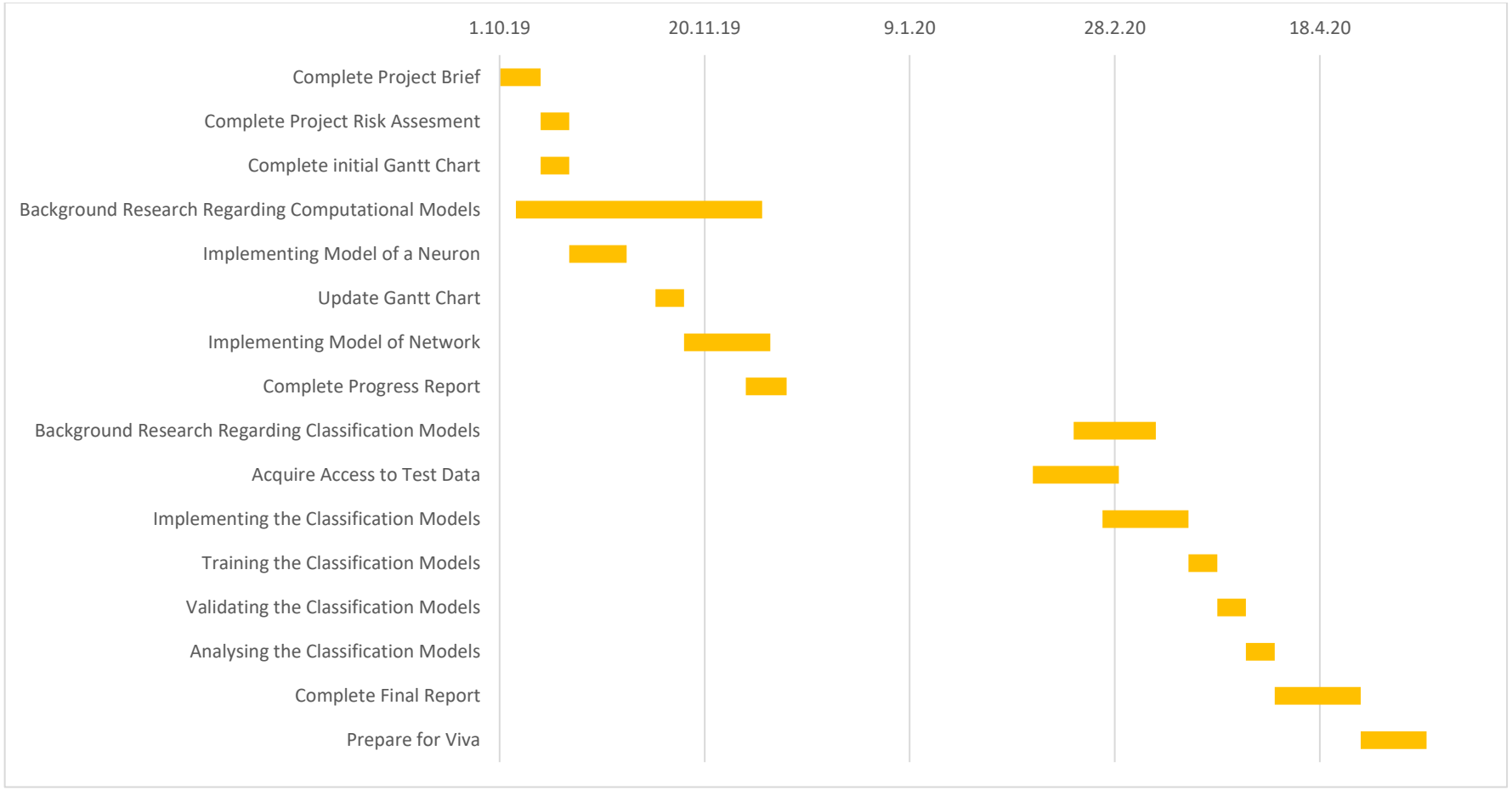

Figure 30: Initial Gantt Chart

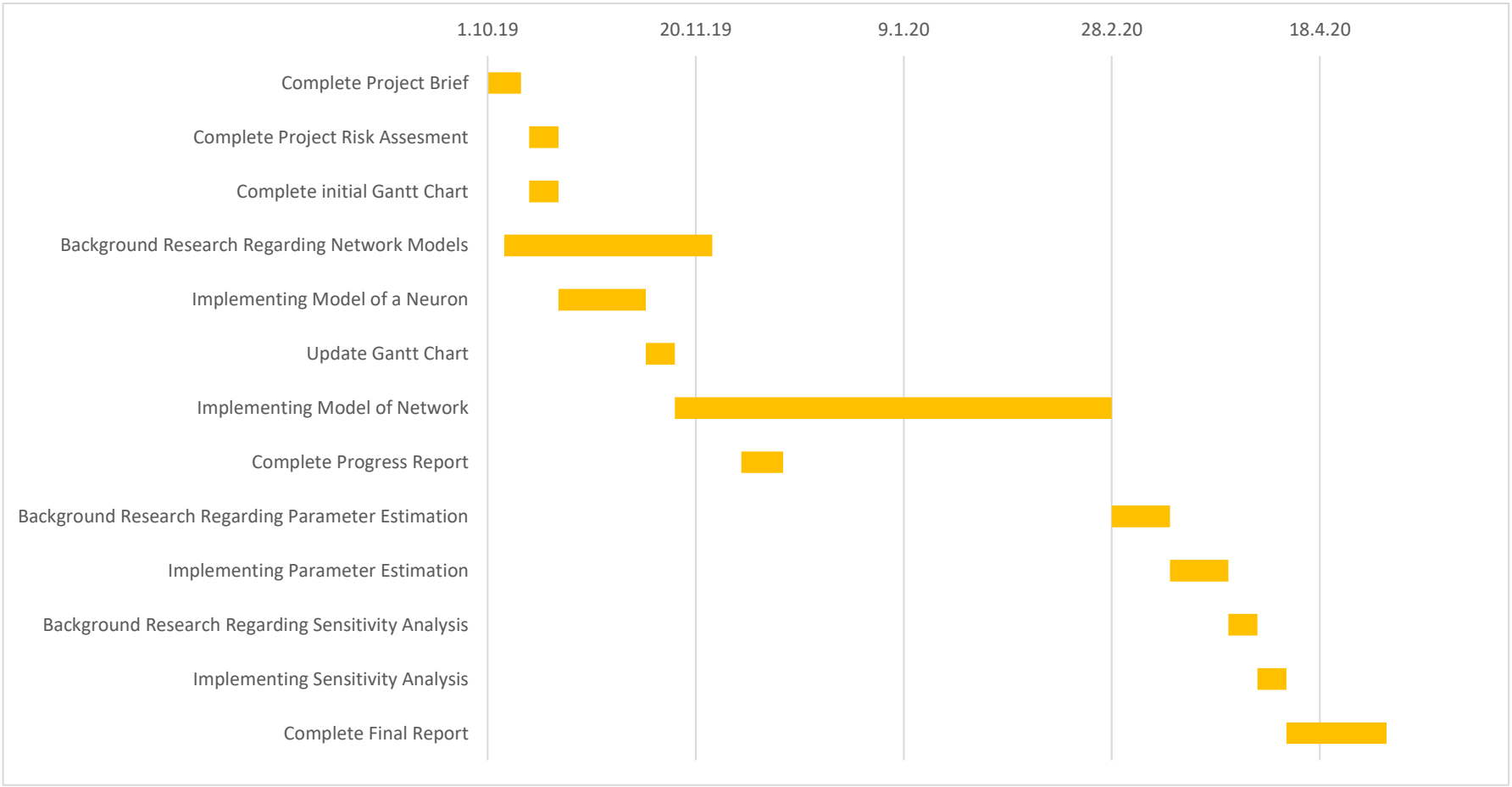

Figure 31: Executed Project Schedule

Appendix C- Risk Assessment

PART A									
(1) Risk identification		**(2) Risk assessment**							**(3) Risk management**
Risk	**Potential Consequences**	**Inherent**			**Control measures**	**Residual**			**Further controls**
		Likelihood	**Impact**	**Score**		**Likelihood**	**Impact**	**Score**	
Loss of Work	Failure	3	5	15	Use of cloud storage to back-up work and allow access to work from other machines	1	5	5	Back-up project work on a removable storage device
Illness	Delay to Schedule	3	3	9	Allow plenty of time to complete each task- this will reduce the impact of short-term illnesses	3	2	6	Exercise regularly
Missed Deadlines	Failure/Lose Marks	2	5	10	Check project schedule during weekly supervisor meetings	1	5	5	Refer to coursework deadlines on ECS student intranet
Change of Plan	Delay to Schedule	4	2	8	Regularly re-evaluate project schedule	4	1	4	Discuss project schedule with supervisor
Unable to Access Test Data	Can't Train Classification Models- No way of Assessing Models	4	4	16	Have method of generating synthetic data	4	1	4	Contact researcher as early as possible to prevent slow communications delaying project
Lack of Computing Power	Delay to Schedule	3	3	9	Apply in advance for access to University's high-performance computer	3	1	3	Use Julia box for running scripts

Table 4: Reproduced from University of Southampton's student union

Assessment Guidance

1. Eliminate	Remove the hazard wherever possible which negates the need for further controls	If this is not possible then explain why
2. Substitute	Replace the hazard with one less hazardous	If not possible then explain why
3. Physical controls	Examples: enclosure, fume cupboard, glove box	Likely to still require admin controls as well
4. Admin controls	Examples: training, supervision, signage	
5. Personal protection	Examples: respirators, safety specs, gloves	Last resort as it only protects the individual

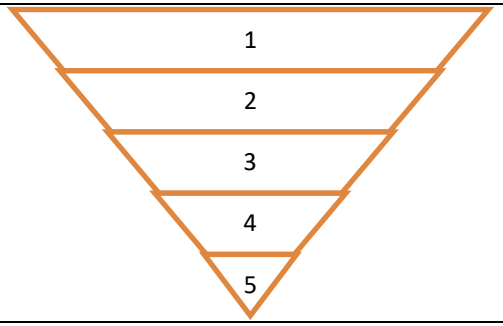

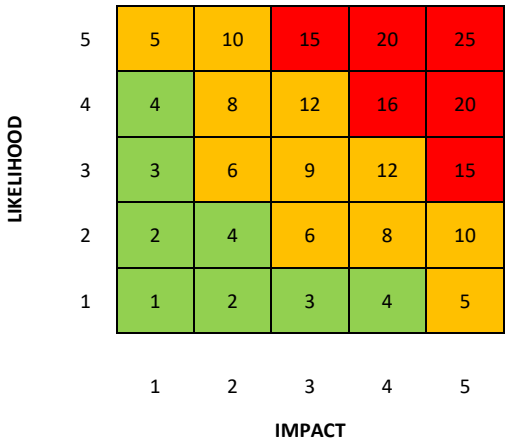

Risk process

1. Identify the impact and likelihood using the tables above.
2. Identify the risk rating by multiplying the Impact by the likelihood using the coloured matrix.
3. If the risk is amber or red – identify control measures to reduce the risk to as low as is reasonably practicable.
4. If the residual risk is green, additional controls are not necessary.
5. If the residual risk is amber the activity can continue but you must identify and implement further controls to reduce the risk to as low as reasonably practicable.
6. If the residual risk is red do not continue with the activity until additional controls have been implemented and the risk is reduced.
7. Control measures should follow the risk hierarchy, where appropriate as per the pyramid above.
8. The cost of implementing control measures can be taken into account but should be proportional to the risk i.e. a control to reduce low risk may not need to be carried out if the cost is high but a control to manage high risk means that even at high cost the control would be necessary.

Impact		Health & Safety
1	Trivial - insignificant	Very minor injuries e.g. slight bruising
2	Minor	Injuries or illness e.g. small cut or abrasion which require basic first aid treatment even in self-administered.
3	Moderate	Injuries or illness e.g. strain or sprain requiring first aid or medical support.
4	Major	Injuries or illness e.g. broken bone requiring medical support >24 hours and time off work >4 weeks.
5	Severe – extremely significant	Fatality or multiple serious injuries or illness requiring hospital admission or significant time off work.

Likelihood	
1	Rare e.g. 1 in 100,000 chance or higher
2	Unlikely e.g. 1 in 10,000 chance or higher
3	Possible e.g. 1 in 1,000 chance or higher
4	Likely e.g. 1 in 100 chance or higher
5	Very Likely e.g. 1 in 10 chance or higher